Molecular Pharmacology Fast Forward. Published on March 13, 2015 as DOI: 10.1124/mol.114.096925
This article has not been copyedited and formatted. The final version may differ from this version.

MOL #96925

Title Page

The molecular basis of oligomeric organization of the human M_3 muscarinic acetylcholine receptor

María José Varela Liste, Gianluigi Caltabiano, Richard J. Ward, Elisa Alvarez-Curto, Sara Marsango and Graeme Milligan

Molecular Pharmacology Group, Institute of Molecular, Cell and Systems Biology, College of Medical, Veterinary and Life Sciences, University of Glasgow, Glasgow G12 8QQ, Scotland, United Kingdom (MJVL, GC, RJW, EA-C, SM, GM), and Laboratori de Medicina Computacional, Unitat de Bioestadística, Facultat de Medicina, Universitat Autònoma de Barcelona, 08193 Bellaterra, Spain (GC)

Molecular Pharmacology Fast Forward. Published on March 13, 2015 as DOI: 10.1124/mol.114.096925
This article has not been copyedited and formatted. The final version may differ from this version.

MOL #96925

Running title page:

Organization of muscarinic receptor oligomers

To whom correspondence should be addressed: Graeme Milligan, Wolfson Link Building 253, University of Glasgow, Glasgow G12 8QQ, Scotland, U.K. Tel +44 141 330 5557, FAX +44 141 330 5481, e-mail: Graeme.Milligan@glasgow.ac.uk or Gianluigi Caltabiano, Unitat de Bioestadística, Facultat de Medicina, Universitat Autònoma de Barcelona, 08193 Bellaterra, Spain, e-mail: gianluigicaltabiano@gmail.com

Manuscript information

Text Pages:	54
Tables:	0
Figures:	13
Words in Abstract:	**248**
Words in Introduction:	**762**
Words in Discussion:	**2709**
References	**58**

Molecular Pharmacology Fast Forward. Published on March 13, 2015 as DOI: 10.1124/mol.114.096925
This article has not been copyedited and formatted. The final version may differ from this version.

Non-standard Abbreviations

DDM, n-dodecyl-β-D-maltoside; EGF, Epidermal Growth Factor; ER, endoplasmic reticulum; FRET, Fluorescence Resonance Energy Transfer; GPCR, G protein-coupled receptor, htrFRET, homogeneous time-resolved Fluorescence Resonance Energy Transfer; hM_3R, human muscarinic M_3 receptor; PNGaseF, N-glycosidase F; PBS, phosphate buffered saline; PEI, polyethylenimine;

Molecular Pharmacology Fast Forward. Published on March 13, 2015 as DOI: 10.1124/mol.114.096925
This article has not been copyedited and formatted. The final version may differ from this version.

Abstract

G protein-coupled receptors, including the M_3 muscarinic acetylcholine receptor, can form homo-oligomers. However, the basis of these interactions and the overall organizational structure of such oligomers are poorly understood. Combinations of site-directed mutagenesis and homogenous time-resolved FRET studies that assessed interactions between receptor protomers at the surface of transfected cells indicated important contributions of regions of transmembrane domains I, IV, V, VI and VII, as well as intracellular helix VIII, to the overall organization. Molecular modelling studies based on both these results and an X-ray structure of the inactive state of the M_3 receptor bound by the antagonist/inverse agonist tiotropium were then employed. The results could be accommodated fully by models in which a proportion of the cell surface M_3 receptor population is a tetramer with rhombic, but not linear, orientation. This is consistent with previous studies based on spectrally-resolved, multi-photon FRET. Modelling studies suggest, furthermore, an important role for molecules of cholesterol at the dimer + dimer interface of the tetramer, consistent with the presence of cholesterol at key locations in many G protein-coupled receptor crystal structures. Mutants that displayed disrupted quaternary organization were often poorly expressed and showed immature N-glycosylation. Sustained treatment of cells expressing such mutants with the muscarinic receptor inverse agonist atropine increased cellular levels and restored both cell surface delivery and quaternary organization to many of the mutants. These observations suggest that organization as a tetramer may occur before plasma membrane delivery and may be a key step in cellular quality control assessment.

Molecular Pharmacology Fast Forward. Published on March 13, 2015 as DOI: 10.1124/mol.114.096925
This article has not been copyedited and formatted. The final version may differ from this version.

Introduction

G protein-coupled receptors (GPCRs) constitute the largest family of plasma membrane spanning polypeptides. They play pivotal roles in cell signalling and in the regulation of biological processes and are privileged drug targets. The muscarinic receptors are a family (M_1-M_5) of GPCRs that respond to the neurotransmitter acetylcholine (Wess, 1996, Kruse et al., 2014). The M_3 receptor is involved in numerous important physiological functions. These include maintaining normal blood glucose levels by regulating insulin secretion (Ruiz de Azua et al., 2012, Nakajima et al., 2013) and the control of the salivary response (Ehlert et al., 2012, Sumida et al., 2013). Such functions reflect preferential activation of G proteins of the G_q family (Wess, 1996, Kruse et al., 2014).

GPCRs were initially thought to exist and function exclusively as monomeric entities. However, evidence accumulated over the past two decades indicates that they may also form and function, at least in part, as dimers or higher-order oligomers (Milligan, 2004, 2013, Ferre et al., 2014). The implications of such protein-protein interactions for regulating receptor trafficking and ligand pharmacology have been widely considered in recent times (Milligan, 2009, Lohse, 2010). Despite this, identification of the structural elements governing the dimerization/oligomerization of this class of receptors has been challenging (Milligan, 2013, Ferre et al., 2014). An understanding of the basis of such interactions is essential to better understand how GPCRs function at the molecular level. Such knowledge may provide new approaches to modulate GPCR oligomerization for therapeutic purposes.

A series of studies have demonstrated the capacity of monomers of muscarinic receptor subtypes to self-associate in both living cells (Goin and Nathanson, 2006, Alvarez-Curto et al, 2010b) and following purification and reconstitution (Ma et al., 2007, Redka et al., 2014). Many of these studies have assumed that the major organizational structure of such complexes is as a dimer or have been unable to discriminate between the presence of dimers and higher-order organization. However,

Molecular Pharmacology Fast Forward. Published on March 13, 2015 as DOI: 10.1124/mol.114.096925
This article has not been copyedited and formatted. The final version may differ from this version.

recent studies based on the guanine nucleotide sensitivity of ligand binding to M_2 muscarinic receptors in both reconstituted systems and in native sarcolemmal membranes are consistent with the receptor existing and functioning as a tetramer (Redka et al., 2014). Moreover, via application of spectrally-resolved, multi-photon fluorescence resonance energy transfer (FRET), Patowary et al., (2013) recently identified the predominant oligomeric form of the human M_3 muscarinic receptor (hM_3R) expressed in a HEK293 derived cell line as a tetramer, and that this exists in equilibrium with dimeric species. Atomic level structures of the μ-opioid receptor (Manglik et al., 2012) and the turkey β_1-adrenoceptor (Huang et al., 2013) have identified both a potential protein-protein interface involving residues from each of transmembrane domain (TMD) I and helix VIII and an interface involving residues from TMD V with residues from either TMD VI (μ-opioid receptor) or TMD IV (β_1-adrenoceptor). Distinct interfaces on either side of the TMD helix bundle could allow organization as a tetramer (Patowary et al., 2013) and these have been illustrated in a quasi-linear arrangement (Manglik et al., 2012, Huang et al., 2013). By contrast, mathematical analysis of the range of FRET efficiency values obtained by Patowary et al., (2013) was most consistent with the tetrameric form being arranged as a rhombus or parallelogram.

Herein we used mutational studies directed by both a high resolution, inactive state structure of the rat M_3 muscarinic receptor (Kruse et al., 2012) and previous work on 'dimerization' interfaces of the M_3R (McMillin et al., 2011) to explore hM_3R receptor interaction interfaces at the surface of transfected cells. We have then generated models consistent with the data and used these to suggest further mutational studies to probe the most likely organization of this receptor.

Mutations in multiple TMDs and in the intracellular 'helix VIII' disrupted receptor organization. As well as individual dimer forms, molecular models based on these results are consistent with organization as dimer + dimer to generate a 'rhombic' tetramer. However, the results are not consistent with the 'linear' tetramers predicted from X-ray structures of various rhodopsin-family GPCRs. The results obtained are also compatible with significant roles for molecules of cholesterol in providing the dimer + dimer interface, rather than interactions being limited to direct

Molecular Pharmacology Fast Forward. Published on March 13, 2015 as DOI: 10.1124/mol.114.096925
This article has not been copyedited and formatted. The final version may differ from this version.

protein-protein interactions. A number of the mutated forms of the receptor which were compromised in their ability to effectively generate organizational structure were also poorly delivered to the surface of transfected cells. A muscarinic receptor inverse agonist promoted cell surface delivery and restored wild type organization of many of these. This is consistent with the formation of receptor oligomers at an early stage of synthesis and prior to cell surface delivery.

Materials and Methods

Materials for tissue culture were from Sigma-Aldrich® (Poole, Dorset, UK), GE Healthcare (Little Chalfont, Buckinghamshire, UK) or Invitrogen™ (Paisley, UK). Rabbit polyclonal anti-SNAP tag antiserum was from New England BioLabs® Inc. (Hitchin, UK). Anti-rabbit secondary IgG horseradish peroxidase-linked antibody was from GE Healthcare (Little Chalfont, Buckinghamshire, UK). Mouse monoclonal anti-α-tubulin antiserum was from Sigma-Aldrich® (Poole, Dorset, UK). Anti-mouse secondary IgG horseradish peroxidase-linked antibody was from GE Healthcare (Little Chalfont, Buckinghamshire, UK). Hoechst 33342 trihydrochloride trihydrate was from Life Technologies (Paisley, UK). Oligonucleotides were from Thermo Fisher Scientific (Loughborough, UK) or Eurofins Genomics (Acton, London, UK). n-Dodecyl β-D-maltoside (DDM) and atropine were from Sigma-Aldrich® (Poole, Dorset, UK). NuPAGE® Novex® 4-12% Bis-Tris Gels, NuPAGE® MOPS SDS running buffer and NativePAGE™ Novex® 3-12% Bis-Tris gels were purchased from Life Technologies™ (Paisley, UK). Tag-lite® reagents were supplied by Cisbio Bioassays (Bagnols, Ceze, France). Complete™ protease inhibitor cocktail tablets, N-glycosidase F (PNGase) and DpnI restriction enzyme were from Roche Diagnostics (Burgess Hill, UK). [^{3}H]N-methylscopolamine ([^{3}H]NMS) was from Perkin-Elmer.

Molecular Pharmacology Fast Forward. Published on March 13, 2015 as DOI: 10.1124/mol.114.096925
This article has not been copyedited and formatted. The final version may differ from this version.

DNA constructs and mutant receptors

The plasmid pSEM1-26 m (SNAP tag), as supplied by Covalys Biosciences AG/New England Biolabs (Hitchin, UK), was modified by the addition of a small linker region encoding the metabotropic glutamate receptor 5 signal sequence (MVLLLILSVLLLKEDVRGSAQS) and the VSV-G epitope tag (YTDIEMNRLGK) between the *Cla1* and *EcoR1* sites of the multiple cloning site upstream of the SNAP tag (MCS1). The human muscarinic M_3 receptor (hM_3R) was PCR amplified using primers designed to add *BamH1* and *Not1* sites to the fragment termini and then ligated into the multiple cloning site downstream of the SNAP tag (MCS2) of the modified plasmid (Alvarez-Curto et al., 2010). This construct was used as template to generate various mutants by alanine substitution mutagenesis using the QuikChange method (Stratagene, Agilent Technologies, Santa Clara, CA). Complementary primers containing the desired mutation flanked by at least 9 bases of wild type sequence on either side were used in the mutagenic PCR reactions. PCR reaction mixture was digested with DpnI to remove the template DNA and leave only the newly synthesized double-stranded mutant construct, which was then transformed into a suitable bacterial host. The entire coding sequences of all mutant hM_3 constructs were confirmed by sequencing.

Cell culture and transient transfection of HEK 293T cells

Human embryonic kidney (HEK) 293T cells were maintained in Dulbecco's Modified Eagle's Medium supplemented with 0.292 g/l L-glutamine, 100u.ml^{-1} penicillin, 0.1mg.ml^{-1} streptomycin mixture and 10 % heat-inactivated fetal bovine serum (FBS) at 37°C in a 5%

Molecular Pharmacology Fast Forward. Published on March 13, 2015 as DOI: 10.1124/mol.114.096925
This article has not been copyedited and formatted. The final version may differ from this version.

CO_2 humidified atmosphere. Cells were grown to 60 to 80% confluence in 60 mm dishes before transient transfection. For all experiments, transfections were performed with polyethylenimine (PEI) (Fluka Analytical, Poole, Dorset, UK). For htrFRET studies, a range of amount of DNA (0-2.5 µg) was combined with PEI (ratio 1:6) in 250 µl of 150 mM NaCl solution, thoroughly mixed and incubated for 10 min at room temperature. Cell medium was changed and the DNA-PEI mixture added to the cells medium in a drop-wise manner.

Cell treatments

For atropine treatment transfected cells were incubated with 10 µM atropine for 24 h.

[^{3}H]N-methylscopolamine binding assays

HEK293T cells transiently transfected with varying amounts (0-2.5 µg) of plasmid encoding VSV-SNAP-hM_3R were grown overnight on white 96 well microtiter plates which had been treated with 0.1 mg.ml^{-1} poly-D-lysine. The medium was removed and replaced with 100 µl per well cold phosphate buffered saline (PBS)(137 mM NaCl, 2.7 mM KCl, 1.5 mM KH_2PO_4, 8 mM Na_2HPO_4 , pH 7.4) containing 1 nM [^{3}H]-NMS. Non-specific binding was determined in the presence of 10 µM atropine. The plates were incubated at 4°C for 150 min and the assay terminated by removal of the binding cocktail, followed by washing with 4x100 µl per well, ice-cold 1x PBS. 100 µl per well Microscint 20 was added and the plates sealed before overnight incubation at room temperature on a rapidly shaking platform. Bound ligand was determined using a Packard Topcount NXT. Using the specific binding per well and the number of cells per well, receptor copies per cell was determined.

Cell lysates and western blotting Cells were washed once and harvested in cold phosphate buffered saline (PBS) (137 mM NaCl, 2.7 mM KCl, 1.5 mM KH_2PO_4, 8 mM Na_2HPO_4 , pH 7.4) and incubated in lysis buffer (150 mM NaCl, 0.01 mM Na_3PO_4, pH 7.4, 2 mM EDTA,

Molecular Pharmacology Fast Forward. Published on March 13, 2015 as DOI: 10.1124/mol.114.096925
This article has not been copyedited and formatted. The final version may differ from this version.

0.5% n-dodecyl β-D-maltoside (DDM) and 5% glycerol) supplemented with Complete™ protease inhibitor cocktail tablets (Roche Diagnostics) on a rotating wheel for 1 h at 4°C. Samples were then centrifuged at 4°C for 15 min at 14000 x g and the supernatant was placed into a fresh tubes. Laemmli loading buffer was added and samples were heated at 65°C for 5 min and subjected to SDS-PAGE analysis using NuPAGE® Novex® 4-12% Bis-Tris Gels and MOPS SDS running buffer (Life Technologies). After electrophoresis, proteins were transferred onto nitrocellulose membrane which was then incubated in 5% fat-free milk in PBS containing 0.1% Tween20 at 4°C overnight on a rotating shaker to block non-specific binding sites. The membrane was incubated for 4 h at room temperature with a polyclonal anti-SNAP tag antiserum diluted 1:2000, washed and subsequently incubated with a horseradish peroxidase-linked anti-rabbit IgG secondary antibody (diluted 1:10000) for 2 h at room temperature.

Immunoblots were developed by the application of enhanced chemiluminescence solution (Pierce Chemical, Rockford IL) according to the manufacturer's instructions. Membrane were stripped using standard protocol from Abcam and reprobed with anti-α-tubulin antiserum diluted 1:5000 for 4 h at room temperature, washed and subsequently incubated with a horseradish peroxidase-linked anti-mouse IgG secondary antibody (diluted 1:20000) for 2 h at room temperature, before being developed as above.

Treatments of cell lysates

Deglycosylation was performed using N-glycosidase F (PNGaseF) at a final concentration of 0.05 unit/µl for 2 h at 37°C.

Blue Native-PAGE

Molecular Pharmacology Fast Forward. Published on March 13, 2015 as DOI: 10.1124/mol.114.096925
This article has not been copyedited and formatted. The final version may differ from this version.

Cells transfected transiently with the appropriate plasmid were harvested in PBS and lysed in lysis buffer (150 mM NaCl, 0.01 mM Na_3PO_4, pH 7.4, 2 mM EDTA, 0.5% DDM and 5% glycerol) supplemented with Complete™ protease inhibitor cocktail tablets on a rotating wheel for 1 h at 4°C. Samples were then centrifuged at 4°C for 15 min at 14000 x g and the supernatant was transferred to fresh tubes. A total of 18 µg of solubilized supernatant plus 4 µl of G250 additive (Life Technologies) was loaded into each lane of NativePAGE™ Novex® 3-12% Bis-Tris Gels (Life Technologies). In certain samples 1% (w/v) SDS was added and incubated for 10 min at room temperature prior to the addition of G250 additive and loaded onto the gel. After electrophoresis, proteins were transferred (90 min at 25 V) onto a PVDF membrane that had been pre-wetted for 30 sec in methanol. The membrane was then fixed in 8% acetic acid for 15 min and blocked with 5% fat-free milk in PBS containing 0.1% Tween20 at 4°C overnight on a rotating shaker. The membrane was then probed with anti-SNAP antibody and developed as described above.

Homogeneous time-resolved fluorescence resonance energy transfer (htrFRET) studies

Cells expressing the receptor variant of interest were seeded at 30000 cells/well in solid black 96-well plates (Greiner Bio-One Ltd, Stonehouse, UK) pretreated with 0.1 mg/ml poly-D-lysine. The growth medium was replaced with 40 µl containing a pre-determined optimal mixture of donor and acceptor, Tag-lite™ SNAP-Lumi4Tb (10 nM) and Tag-lite™ SNAP-Red (100 nM) in labelling medium (Cisbio Bioassays, Bagnols, Ceze, France). Plates were incubated for 1 h at 37°C in 5% CO_2 in a humidified atmosphere and washed four times in Hanks Balanced Salt Solution (HBSS). 100 µl of labelling medium was added to each well, and the plates were read using a PHERAstar FS reader (BMG Labtech Ltd, Aylesbury, UK).

Molecular Pharmacology Fast Forward. Published on March 13, 2015 as DOI: 10.1124/mol.114.096925
This article has not been copyedited and formatted. The final version may differ from this version.

After excitation at 337 nm, both the emission signal from the Tag-lite™ SNAP-Lumi4 Tb cryptate (620 nm) and the htrFRET signal resulting from the acceptor Tag-lite™ SNAP-Red (665 nm) were recorded.

To determine cell surface receptor levels the growth medium was replaced with 50 µl fresh medium containing 10 µg/ml of the nuclear DNA-binding dye Hoechst 33342 (Life Technologies). Following incubation at 37°C for 20 min, the Hoechst stain was removed and the wells washed with 100 µl per well warm growth medium. 40 µl of 10 nM donor alone (Tag-lite™ SNAP-Lumi4Tb) in labelling medium was added. Plates were incubated for 1 h at 37°C in 5% CO_2 in a humidified atmosphere and subsequently washed four times in HBSS. 100 µl of labelling medium was added to each well and after excitation at 337 nm, fluorescent emission at 620 nm was measured. Subsequently, Hoechst staining was measured at 460 nm using a POLARstar microplate reader (BMG Labtech Ltd). The fluorescent emission at 620 nm was corrected for cell number using the Hoechst staining values.

Computational methods

Modeller 9v8 (Marti-Renom et al., 2000) was used to model the hM_3R receptor using the structure of the rat M_3R bound to the antagonist tiotropium as template (PDB code: 4DAJ) (Kruse et al., 2012). hM_3R helix VIII was modelled as being four residues (one helix turn) longer than observed in the rat M_3R crystal structure to extend to the cysteine residue (position location 8.60) that is predicted to terminate helix VIII and which in many receptors is modified by acylation. All released structures featuring cholesterol molecules ($ß_2$-adrenoceptor, serotonin 5-HT_{2B} receptor, adenosine A_{2A} receptor, µ-opioid receptor and the recently resolved $P2Y_{12}$ receptor) were superposed with the hM_3 model and the cholesterol(s)

Molecular Pharmacology Fast Forward. Published on March 13, 2015 as DOI: 10.1124/mol.114.096925
This article has not been copyedited and formatted. The final version may differ from this version.

extracted and added to hM_3R models at the equivalent positions of the structure. Dimers of hM_3R with an interface including TMD I were constructed based on those observed in the 'dimer' crystal structures of the inactive, mutationally stabilized turkey β_1-adrenoceptor (PDB code: 4GPO) (Huang et al., 2013). The same template structure was used to build dimers of hM_3R with an interface including TMD IV. In the latter case, the rM_3R crystal structure shows internal loop 2 to be bent strongly outwardly (Kruse et al., 2012) and a simple superimposition of hM_3R protomers onto a model of the turkey β_1-adrenoceptor TDM IV-TMD IV dimer (Huang et al., 2013) leads to a steric clash between these loops. Monomers were withdrawn along an axis perpendicular to the interaction surface, until steric collisions were removed. This prevents R5.60 from being involved in an active TMD IV-mediated dimer interface, as observed in the turkey β_1-adrenoceptor. Tetramer models were built as the result of dimer+dimer associations. Dimers were arranged manually as rigid bodies, initially based on overall complementarity of shape of their Van Der Waals surfaces to maximize the buried interface and to avoid contacts between helices. The models were then manually refined based on experimental data from the mutagenesis studies. Dimers and dimer+dimer models, and potential cholesterol molecules bound to them, were energy minimized with restraints on backbone atoms, using gromacs4.6 (Hess et al., 2008), to relax side chains and improve inter-monomer residue interactions.

Tetramer models were developed initially on overall complementarity of shape and then refined based on experimental data from the mutagenesis studies. Tetramer models were considered as potentially valid only if they both allowed the simultaneous binding of two heterotrimeric G proteins in their nucleotide-free form, as in the atomic level crystal of the β_2-adrenoceptor complexed with nucleotide free $G\alpha_s$ (PDB code :3sn6) (Rasmussen et al.,

Molecular Pharmacology Fast Forward. Published on March 13, 2015 as DOI: 10.1124/mol.114.096925
This article has not been copyedited and formatted. The final version may differ from this version.

2012) and could account for experimental discrimination (at least simultaneous contribution of the main two "dimeric" interfaces, TMD I/helix VIII and TMD V-TMD V). Modelling figures were generated using PyMOL 1.5.3 (Schrodinger, 2012).

Data analysis

Experiments were performed on at least three independent occasions and analyzed using Prism 5.2 (GraphPad Software). Where appropriate, data are expressed as means ± S.E.M. Statistical analysis was performed by one-way analysis of variance or Student's t- test.

RESULTS

Previous studies on the M_3 muscarinic receptor (M_3R) have shown that mutation of sequences within many of the TMD regions appears to compromise receptor quaternary structure formation or stability (McMillin et al., 2011). Such results have been interpreted as being consistent with the capacity of the receptor to form dimers in a range of ways via a number of distinct interfaces (McMillin et al., 2011, Hu et al., 2012). Recent studies have suggested that rather than being limited to dimers, muscarinic receptors including both the M_2 (Redka et al., 2014) and M_3 (Patowary et al., 2013) subtypes, may form, and potentially function, as tetramers. We, therefore, initiated studies to address such a possibility for structural organization and to assess if previous results (McMillin et al., 2011) would be consistent with such a model.

To explore the contribution of various regions of the sequence of the human (h)M_3R to self-association and organization into dimers and/or higher oligomers we modified this receptor to optimize cell surface delivery in transient transfection studies. These alterations

Molecular Pharmacology Fast Forward. Published on March 13, 2015 as DOI: 10.1124/mol.114.096925
This article has not been copyedited and formatted. The final version may differ from this version.

were also designed to produce a version of the receptor suitable for both immunodetection and to allow covalent attachment of fluorophores to appropriately folded and cell surface-delivered copies of the protein. The first of these requirements was achieved by addition of the signal sequence from the metabotropic glutamate receptor 5 to the extracellular N-terminal domain of the receptor, as we have previously used for a number of other rhodopsin-like GPCRs (Xu et al., 2012). Additional incorporation of the VSV epitope-tag sequence and then the SNAP-tag polypeptide after the signal sequence provided the other two desired features and produced the final 'wild type' construct, VSV-SNAP-hM_3R. This reflects that the N-terminal domain of GPCRs will be extracellular if the protein is correctly delivered to the plasma membrane. Using intact cells, only cell surface copies of the receptor can be labelled, therefore, by SNAP-tag targeted fluorophores (Ward and Milligan, 2014). cDNA encoding VSV-SNAP-hM_3R was transfected transiently into HEK293T cells. Subsequent immunoblotting of SDS-PAGE resolved cell lysates with an anti-SNAP antiserum resulted in detection of the translated products as a group of poorly resolved species (**Figure 1A**). Treatment with PNGaseF showed these to reflect differential extents of N-glycosylation of the receptor polypeptide (**Figure 1A**), in which the predominant forms migrated with apparent molecular mass between 100-120 kDa. Effective cell surface delivery of the VSV-SNAP-hM_3R construct was demonstrated, following addition to intact cells of SNAP-Lumi4Tb, by monitoring fluorescence emission at 620 nm after excitation at 337 nm (**Figure 1B**). This fluorophore binds covalently to the SNAP tag within the extracellular N-terminal domain of the receptor construct in a 1:1 ratio. Increasing levels of 620 nm emission and, therefore, cell surface receptor per cell were recorded as the amount of transfected cDNA was increased (**Figure 1B**). Levels of cell surface VSV-SNAP-hM_3R expression were

Molecular Pharmacology Fast Forward. Published on March 13, 2015 as DOI: 10.1124/mol.114.096925
This article has not been copyedited and formatted. The final version may differ from this version.

quantified by the specific binding of the cell impermeant, muscarinic antagonist [^{3}H]-NMS. This also increased with amount of cDNA transfected and corresponded to some 20,000 to 200,000 copies per cell over the range of cDNA amounts used (**Figure 1C**). Demonstration that the receptor construct was forming dimeric/oligomeric complexes at the surface of the cells was produced by co-addition to intact cells of a single concentration of SNAP-Lumi4Tb, as energy donor, and varying concentrations of SNAP-Red, as energy acceptor. This resulted in a bell-shaped distribution of resonance energy transfer from SNAP-Lumi4Tb to SNAP-Red and subsequent emission at 665 nm, following excitation at 337 nm, in homogenous time-resolved (htr)FRET experiments (**Figure 1D**). This outcome was anticipated because competition between the energy donor and acceptor to covalently label the available SNAP-tag containing cell surface hM_3R population eventually results in the energy acceptor out-competing the energy donor. This limits resonance energy transfer at high acceptor concentrations (Ward and Milligan, 2014). Importantly, such preliminary experiments also identified the optimal ratio of SNAP-Lumi4Tb to SNAP-Red to maximize receptor-receptor htrFRET signals for subsequent studies (**Figure 1D**). To define that the htrFRET output at 665 nm actually reported hM_3R-hM_3R interactions and not simply protein-protein proximity because of the amount of receptor expressed, we employed the single TMD Epidermal Growth Factor (EGF) receptor. In the absence of agonist activation this receptor is almost entirely monomeric. The extracellular N-terminal region of this receptor was also modified to incorporate both the VSV- and SNAP-tags. Transient transfection was optimized to achieve a similar cell surface expression level of this construct as for VSV-SNAP-hM_3R, measured by emission at 620 nm following addition of SNAP-Lumi4Tb (**Figure 1D insert**). However, now, co-addition of a range of concentrations of SNAP-Red resulted in very little energy transfer (**Figure 1D**).

Molecular Pharmacology Fast Forward. Published on March 13, 2015 as DOI: 10.1124/mol.114.096925
This article has not been copyedited and formatted. The final version may differ from this version.

Biochemical analysis also indicated that VSV-SNAP-hM_3R was present within oligomeric complexes. Addition of DDM extracts of lysates of VSV-SNAP-hM_3R expressing cells to non-denaturing Native Blue PAGE resulted in resolution and detection of high molecular mass, apparently higher-order complex species of VSV-SNAP-hM_3R (**Figure 1E**). As also shown previously for a related hM_3R construct (Milligan, 2013), these oligomeric forms were separated into differentially N-glycosylated forms of monomeric VSV-SNAP-hM_3R when SDS (1% (w/v)) was added to the samples prior to addition to the Native Blue gel (**Figure 1E**). This indicates that the higher-order complexes were not covalently-linked adducts and did not represent irreversibly aggregated protein. Importantly, over the full range of cDNA amounts employed, the level of cell surface receptor oligomers, detected as htrFRET output at 665 nm after co-addition of the optimal ratio of SNAP-Lumi4Tb and SNAP-Red, increased in a linear manner with the amount of cell surface delivered receptor as measured by fluorescence emission at 620 nm (**Figure 1F**).

To identify TMD and/or helix VIII residues involved in hM_3R homomeric interactions the VSV-SNAP-hM_3R construct was used as template to generate a series of variants by alanine mutagenesis (**Figure 2**). These ranged from forms that mutated a pair of amino acids to more extensive alterations involving concurrent replacement of up to four distinct residues. Residues mutated within these regions were selected based, in part, on inspection of the atomic level structure of the rat M_3 receptor bound by the high affinity antagonist/inverse agonist tiotropium (Kruse et al., 2012). Initially, we assessed cell surface delivery of the mutant receptors by emission at 620 nm after excitation at 337 nm in transiently transfected HEK293T cells that were incubated with SNAP-Lumi4Tb (**Figure 3A**). The majority of the mutants displayed reduced, and in some cases very poor, delivery to the cell surface compared to the wild type VSV-SNAP-hM_3R sequence (**Figure 3A**).

Molecular Pharmacology Fast Forward. Published on March 13, 2015 as DOI: 10.1124/mol.114.096925
This article has not been copyedited and formatted. The final version may differ from this version.

Furthermore, as also noted by others (McMillin et al., 2011), the mutants that displayed the poorest cell surface delivery also showed poor levels of the mature, more fully N-glycosylated and, therefore, lower mobility species. In such cases the bulk of the immunodetected protein of these mutants was a poorly N-glycosylated, approximately 85 kDa form (**Figures 3B, 3C**). Indeed, in examples such as the TMD VI mutant I502A,I509A,V513A,F516A VSV-SNAP-hM_3R and the TMD VII mutant F525A,L528A,L532A,I535A VSV-SNAP-hM_3R, where cell surface delivery was almost extinguished, this 85 kDa species was the only form of the receptor construct detected by the anti-SNAP antiserum (**Figure 3C**).

Although many of the mutants were expressed modestly at the cell surface compared to the wild type receptor when using the same amount of cDNA, for each mutant the level of cell surface delivery per cell also increased in a linear manner with increasing amount of cDNA used for transfection. Therefore, by employing a range of amounts of cDNA, direct comparisons of the effectiveness of interactions of the mutated receptors could be made with wild type at equal cell surface expression levels. This was achieved by measuring the slope of the linear regression of the line for htrFRET signal at 665 nm versus expression level, measured as the signal at 620 nm following addition of only SNAP-Lumi4Tb, and comparing this for each individual mutant to data produced for wild type VSV-SNAP-hM_3R in parallel studies (see **Figure 4** for the entire data set).

Both in previous mutagenesis studies of the hM_3R (McMillin et al., 2011) and in X-ray structure 'dimer' interfaces for the β_1-adrenoceptor (Huang et al., 2013) and the μ-opioid receptor (Manglik et al, 2012), residues near the cytoplasmic face of TMD V are indicated to play important roles in receptor-receptor interactions. Herein, concerted mutation to alanine

Molecular Pharmacology Fast Forward. Published on March 13, 2015 as DOI: 10.1124/mol.114.096925
This article has not been copyedited and formatted. The final version may differ from this version.

of W252, R253 and Y255 (residue positions 5.59, 5.60 and 5.62 in the Ballesteros and Weinstein (1995) positioning system) located at the intracellular end of TMD V (**Figure 5A**) generated a form of the receptor that was poorly expressed at the cell surface compared to wild type. However, this mutant was still able to produce homomeric interactions, as assessed by htrFRET emission at 665 nm after co-addition of SNAP-Lumi4Tb and SNAP-Red (**Figure 5B**). These interactions were significantly (**Figure 4)** reduced (**Figure 5B**), however, compared to wild type. Limiting the TMD V mutations to only W252A and R253A resulted in a mutant that was better expressed at the cell surface than W252A,R253A,Y255A VSV-SNAP-hM_3R (**Figures 3A, 3B, 5B**) but which was equally as compromised in oligomeric interactions as W252A,R253A,Y255A VSV-SNAP-hM_3R (**Figure 4, Figure 5B**). These results demonstrate, as indicated previously (McMillin et al., 2011), an important role of this region in hM_3R homomeric interactions.

Equivalent studies were performed for all the other mutants detailed in **Figure 2**. Combined mutation of I502A and I509A (residues 6.46 and 6.53), or of V513A and F516A (residues 6.57 and 6.60) in TMD VI, produced forms of VSV-SNAP-hM_3R that each had major defects in oligomeric interactions (**Figure 4**, **Figure 6A**). Moreover, both were markedly compromised in cell surface delivery (**Figure 3**). Combining these mutations resulted in a version of the receptor that was immature, lacked significant N-glycosylation and was very poorly expressed at the cell surface (**Figure 3**). However, to the extent that htrFRET signals could be measured at the cell surface for this mutant (**Figure 6A**), it appeared to be no more greatly compromised in receptor-receptor interactions than either of the two double mutants that were combined to generate this form (**Figure 6**A, see **Figure 4** for quantification). Mutations introduced in TMD VII between amino acids 525 (residue

Molecular Pharmacology Fast Forward. Published on March 13, 2015 as DOI: 10.1124/mol.114.096925
This article has not been copyedited and formatted. The final version may differ from this version.

7.34) and 535 (residue 7.44), upstream of the 'NPXXY' sequence (NPVCY in hM_3R) that is highly conserved in rhodopsin-family GPCRs, were next assessed. F525A,L528A VSV-SNAP-hM_3 behaved in a manner indistinguishable from wild type (**Figure 4**, **Figure 6B**). By contrast L532A,I535A VSV-SNAP-hM_3R was markedly compromised in capacity for oligomeric assembly (**Figure 4**, **Figure 6B**), and poorly expressed and delivered to the cell surface. Unsurprisingly based on these observations, the combined F525A,L528A,L532A,I535A VSV-SNAP-hM_3R was also very poor in expression and oligomeric assembly (**Figure 6B,** see **Figure 4** for quantitative details).

A number of regions within TMD I have been suggested as contributing to potential dimer/oligomer interfaces from each of experimental, structural and computational approaches. Herein, residues within the sequence from Q67 (residue location 1.31) at the extreme extracellular end, to I87 (residue location 1.51) were modified in various combinations. All residues on the outward face of these areas were mutated to assess their potential involvement, as observed in crystals of the μ- (Manglik et al, 2012) and κ- (Wu et al., 2012) opioid receptors and the turkey β_1-adrenoceptor (Huang et al., 2013). Beginning at the extracellular end of TMD I, mutation of residues to produce Q67A,V68A,I71A,L74A VSV-SNAP-hM_3R caused a relatively small, although highly statistically significant (**Figure 4**), effect on receptor organization (**Figure 7A**). Combined alanine mutation of residues V69, F73, I77 and L80, each also lying on the outward facing side of this helix, had no significant effect (**Figure 4**) on oligomeric organization (**Figure 7B**). However, this combination of mutations had a marked effect on construct expression (**Figure 3**). Deconstruction of this variant to generate firstly V69A,F73A VSV-SNAP-hM_3R allowed effective expression and cell surface delivery (**Figure 3**) of a receptor that also behaved as wild type in the

Molecular Pharmacology Fast Forward. Published on March 13, 2015 as DOI: 10.1124/mol.114.096925
This article has not been copyedited and formatted. The final version may differ from this version.

oligomerization assay (**Figure 4**, **Figure 7B**). I77A,L80A VSV-SNAP-hM_3R was expressed as poorly at the cell surface as the quadruple mutant (**Figure 3**) but, again although producing only a modest effect on receptor oligomerization (**Figure 7**B), this was statistically significant (**Figure 4**). By contrast, mutation of residues further down TMD I to produce, L80A,I83A,I84A,I87A VSV-SNAP-hM_3R, had a large effect on both cell surface expression (**Figure 3)** and receptor-receptor interactions at expression levels equal to the wild type receptor construct (**Figure 7C**). Finally in TMD I, concurrent mutation to alanine of only F73 and L80 had, by contrast, no measurable effect on receptor expression (**Figure 3**) or organization (**Figure 4**, **Figure 7D**).

TMD III is rarely implicated as potentially providing residues that contribute to GPCR dimer or oligomer interfaces (Milligan, 2013). We, therefore, generated a mutant within TMD III, L139A,L143A VSV-SNAP-hM_3R, potentially as a control, predicted not to affect hM_3R-hM_3R interactions. However, this mutation was expressed to only very low levels and this precluded further analysis. By contrast TMD IV is often indicated as a potential dimer interface (Milligan, 2013). Indeed, in the case of the M_3R, residues of TMD IV located towards the cytoplasmic face have been shown previously to limit dimeric/oligomeric organization (McMillin et al., 2011). We also generated mutants, therefore, in both this region K183A,R184A,V187A VSV-SNAP-hM_3R and higher up TMD IV, L191A,V194A,I195A,V198A VSV-SNAP-hM_3R. Although L191A,V194A,I195A,V198A VSV-SNAP-hM_3R did not alter oligomeric organization (**Figure 4** and **Figure 8A**), as predicted from previous studies, K183A,R184A,V187A VSV-SNAP-hM_3R displayed markedly reduced interactions (**Figure 4** and **Figure 8B**).

Molecular Pharmacology Fast Forward. Published on March 13, 2015 as DOI: 10.1124/mol.114.096925
This article has not been copyedited and formatted. The final version may differ from this version.

Residues within helix VIII are often noted to contribute to the same receptor-receptor interaction interface as amino acids in TMD I (Milligan, 2013, Ferre et al., 2014). Therefore, residues within the helix VIII section of the C-terminal tail, which runs parallel to the plasma membrane, were altered. Mutation of both L559 (residue location 8.58) and L560 (residue location 8.59) just before the end of this helix (**Figure 9A**) resulted in both reduced expression (**Figure 3**) and markedly reduced oligomer interactions (**Figure 4**, **Figure 9B**). Moreover, mutation of a series of residues located in a region more proximal to TMD VII, to produce F555A,K556A,M557A VSV-SNAP-hM_3R also resulted in a form of the receptor in which more modest, but still significant (**Figure 4**), reduction in the effectiveness of cell surface receptor-receptor interactions was recorded (**Figure 9C**).

A series of studies have indicated that receptor dimerization/oligomerization may occur before membrane delivery, potentially in the endoplasmic reticulum (ER)/Golgi apparatus as part of the quality control of protein folding and maturation (Salahpour et al., 2004, Wilson et al., 2005, Canals et al., 2009, Kobayashi et al., 2009). Many GPCR mutants are incorrectly organized and sent for destruction prior to cell surface delivery. In a number of cases, including receptor variants that appear poorly able to dimerize/oligomerize (Dunham and Hall, 2009, Leidenheimer and Ryder, 2014), pharmacological ligands that can cross cellular membranes are able to bind to the mutant receptor at the ER/Golgi and promote (more) effective folding and subsequent cell surface delivery (Dunham and Hall, 2009, Leidenheimer and Ryder, 2014). Ligands acting in this manner are described as 'pharmacological chaperones' (Dunham and Hall, 2009, Leidenheimer and Ryder, 2014, Petaja-Repo and Lackman, 2014). To assess ligand effects on a number of the mutant forms of VSV-SNAP-hM_3R we employed sustained overnight treatment of HEK293T cells transiently expressing the variant of interest with the prototypic high affinity muscarinic

Molecular Pharmacology Fast Forward. Published on March 13, 2015 as DOI: 10.1124/mol.114.096925
This article has not been copyedited and formatted. The final version may differ from this version.

antagonist/inverse agonist atropine. Even for the wild type VSV-SNAP-hM_3R construct atropine treatment resulted in somewhat higher levels of cell surface receptor as monitored by the binding of SNAP-Lumi4Tb (**Figure 10A**). Moreover, across a range of amounts of cDNA transfected, the slope of the 665 nm htrFRET emission signal against 620 nm cell surface expression levels, was increased (**Figures 10B)**, suggesting closer distance between the energy donor and acceptor forms when the receptor was occupied with this ligand. As shown earlier, the TMD I mutant L80A,I83A,I84A,I87A VSV-SNAP-hM_3R was poorly expressed (**Figure 3**) but, after sustained treatment with atropine, cell surface expression was improved significantly (**Figure 10B**). Notably, moreover, the slope of the 665 nm htrFRET emission signal against 620 nm cell surface expression levels increased markedly for this mutant, to become indistinguishable from wild type (**Figure 10B**). This suggests that following atropine binding the organizational structure of the receptor oligomer of this variant also adopted a state akin to the wild type receptor. Equally, for the TMD V mutant W252A,R253A VSV-SNAP-hM_3R atropine treatment improved cell surface delivery (**Figure 10A**) and improved receptor organizational structure (**Figure 11A**). Analysis across a broad range of the mutants studied indicated that, for the majority, treatment with atropine increased cell surface delivery and improved receptor surface organization to a state akin to wild type (**Figure 11A**). However, this was not universal. For the TMD VI mutants, although V513A,F516A VSV-SNAP-hM_3R displayed this behavior, the more extensive I502A,I509A,V513A,F516A VSV-SNAP-hM_3R mutant did not show this pattern, with no increase in the 665 nm/620 nm slope following treatment with atropine (**Figure 11A**). To explore this further immunoblots of untreated and atropine-treated cells expressing the TMD VI mutants were compared. Interestingly, although the I502A,I509A,V513A,F516A VSV-SNAP-hM_3R mutant displayed no mature protein in the absence of atropine treatment, ligand treatment did result in a

Molecular Pharmacology Fast Forward. Published on March 13, 2015 as DOI: 10.1124/mol.114.096925
This article has not been copyedited and formatted. The final version may differ from this version.

proportion of the receptor now becoming N-glycosylated and the proportion of mature I502A,I509A VSV-SNAP-hM_3R and of V513A,F516A VSV-SNAP-hM_3R was increased (**Figure 11B**). This was also the case for the TMD VII mutant F525A,L528A,L532A,I535A VSV-SNAP-hM_3R (not shown).

The overall data set indicated regions in each of TMD I, TMDIV, TMD V, TMD VI and TMD VII, as well as in helix VIII, that affected receptor homomeric interactions. To consider ways to integrate these results with those of others (Park et al., 2002, McMillin et al., 2011, Patowary et al., 2013) we employed an inactive state X-ray structure of the rat M_3 muscarinic receptor monomer bound by the antagonist tiotropium (Kruse et al., 2012). This was used to generate models of potential dimeric/oligomeric organizational structure that would predict further interfaces and would be consistent with the experimental data set (**Figure 12**). Fitting together crystal structure monomers of the M_3R, based on the dimensions of the protein and complementarity of shape, allowed a tightly packed 'rhombic' tetramer model to be produced (**Figure 12A**). This generated a complex with potential contributions from selected residues of TMDs V, VI and VII at the dimer + dimer interface (**Figure 12A**). Other oligomer models based on a TMD I, TMD II and helix VIII dimer interface could also be generated. These included a 'linear' model (**Figure 12B**) that resulted in further interfaces somewhat akin to those either observed directly or which can be postulated from GPCR crystal structures. It was also possible to generate a 'square' tetramer model (**Figure 12C**) but this resulted in a large gap at the centre of the complex that seemed energetically unlikely. A further feature of the higher-order models based on the TMD I, TMD II and helix VIII dimer interface was that this 'rhombic' model also allowed simultaneous interactions with two heterotrimeric G proteins in their nucleotide-free form (**Supplemental Figure 1**). By contrast, when we attempted to generate 'rhombic' models that required a pivotal role of

Molecular Pharmacology Fast Forward. Published on March 13, 2015 as DOI: 10.1124/mol.114.096925
This article has not been copyedited and formatted. The final version may differ from this version.

TMD V at the interface of each dimeric unit it was not possible to either dock two heterotrimeric G proteins in a manner that avoided steric clashes or could account for the experimental data that allowed discrimination between the models (**Supplemental Figures 1, 2 and 3 and Discussion**).

Discussion

The capacity of class A GPCRs to generate dimers and/or higher-order oligomers is well appreciated (Milligan, 2013, Ferre et al., 2014) as is the potential importance of this for function (Milligan, 2004, 2013, Ferre et al., 2014). However, the basis of how monomers form dimers and, indeed, how dimers might interact to generate higher-order complexes, and the interfaces involved, are a matter of considerable debate (Milligan, 2013, Ferre et al, 2014). Data from Wess and colleagues have shown that the hM_3R can generate sufficiently extensive homomeric interactions to allow capture of dimeric forms via chemical cross-linking (Hu et al., 2012). Mutation across individual TMD regions of this receptor has shown that a number of regions contribute to dimeric or higher-order organization (McMillin et al., 2011). Clearly, there are a number of ways in which such results might be interpreted. One is that dimeric interactions may be able to occur in a number of distinct ways, including via each of TMD V-TMD V, TMD VI-TMD VII, TMD IV-TMD V and TMD I-TMD II interactions (McMillin et al., 2011). Observations that dimer/oligomer interactions of muscarinic receptor subtypes may be transient (Hern et al, 2010, Nenasheva et al., 2013) are certainly consistent with this concept if it reflects predominantly a 'kiss and run' phenomenon (Milligan, 2000). A second interpretation of the results of both Wess and

Molecular Pharmacology Fast Forward. Published on March 13, 2015 as DOI: 10.1124/mol.114.096925
This article has not been copyedited and formatted. The final version may differ from this version.

colleagues (McMillin et al., 2011) and those we report herein, is that the contributions of multiple regions of the receptor to structural organization reflects that higher-order complexes beyond dimers can form. This would require contributions from multiple regions of the receptor and might increase complex stability. It is noteworthy, therefore, that although mutations in a number of regions of the receptor did alter htrFRET signals in a manner consistent with producing changes in the overall organizational structure, no single mutant or set of mutants appeared to prevent receptor-receptor contacts. This was also the case in the studies of McMillin et al., (2011). Within the current studies, and as shown previously for other hM_3R constructs (Milligan, 2013), resolution of cell extracts on non-denaturing gels showed a high proportion of the receptor to be present in larger complexes. These were converted to monomeric forms by pre-addition of SDS. In support of this reflecting non-covalent oligomerization, imaging studies linked to mathematical analysis have suggested that a substantial proportion of the hM_3R can exist as tetramers at the cell surface (Patowary et al., 2013). Moreover, these studies suggested potential dynamic interchange between these tetramers and dimer states (Milligan, 2013, Patowary et al., 2013). This may be relevant to the observations both herein and in the studies of McMillin et al, (2011) of a clear role for amino acids at the cytoplasmic end of TMD IV this is not inherently predicted by the 'rhombic' tetramer models. Organization of other class A GPCRs as tetramers has also been supported by approaches including reconstitution experiments in artificial lipid bilayers (β_2-adrenoceptor)(Fung et al., 2009), chemical cross-linking studies (dopamine D_2)(Guo et al., 2005) and detailed characterization of ligand binding studies (muscarinic M_2) (Park et al., 2002, Redka et al., 2014).

Molecular Pharmacology Fast Forward. Published on March 13, 2015 as DOI: 10.1124/mol.114.096925
This article has not been copyedited and formatted. The final version may differ from this version.

Both 'rhombic' and 'linear' tetramer models of hM_3R that employed an interface involving residues from TMD I and from intracellular helix VIII could be produced. Each of these resulted in a second interface that predicted contributions from residues from TMD V and TMD VI. The most extensive predicted dimer + dimer interface in the 'rhombic' tetramer model involved TMD VI, TMD VII and part of TMD I (**Figure 12**). No role of TMD VII in quaternary structure was implicated from the 'linear' tetramer model, and the same was the case for the outer residues of TMD VI close to TMD VII. This allowed experimental assessment of the 'linear' versus 'rhombic' tetramer models with markedly different predicted outcomes for mutants in TMD VI and TMD VII on htrFRET signals and quaternary structure. Mutations in TMD VII upstream from the 'NPXXY' domain resulted in large effects on htrFRET-detected oligomer organization. Such observations are, at a minimum, consistent with the 'rhombic' tetramer model but not with the 'linear' one. However, despite these experimental results, the X-ray structure of the M_3 receptor shows clearly that TMD VII is a strongly kinked helix and is shaped concavely (Kruse et al., 2012). As such it appears ill suited to make extended, direct protein-protein and helix-helix interactions in either a dimer or a higher-order complex. Furthermore, none of the released crystal structures of GPCR dimers involves TMD VII. However, although the complementarity of the shape of M_3R monomers and dimers allowed construction of conceptual 'rhombic' tetramer models, it should be noted that, although much less obvious and extensive than in the 'square' tetramer model, this organization also resulted in a space between the dimers in the region of the proposed dimer + dimer interface, close to residues from TMD I, TMD VI, TMD VII and helix VIII (**Figure 12**). Such 'protein-only' initial models of receptor organization did not consider possible contributions of lipids. Many released crystal structures of class A GPCRs, including the $ß_2$-adrenoceptor (Cherezov et al., 2007), serotonin $5\text{-}HT_{2B}$ receptor (Wacker et

Molecular Pharmacology Fast Forward. Published on March 13, 2015 as DOI: 10.1124/mol.114.096925
This article has not been copyedited and formatted. The final version may differ from this version.

al., 2013), adenosine A_{2A} receptor (Jaakola et al., 2008), μ-opioid receptor (Manglik et al., 2012) and the $P2Y_{12}$ receptor (Zhang et al., 2014), contain molecules of cholesterol. Moreover, cholesterols are sometimes present at the same positions in different crystals. For example cholesterols at TMD I are observed in both ß$_2$-adrenoceptor (Cherezov et al., 2007) and serotonin 5-HT_{2B} receptor (Wacker et al., 2013) crystals. Equally a cholesterol molecule is positioned at the extracellular side of TMD VI-TMD VII in both adenosine A_{2A} receptor (Jaakola et al., 2008) and μ-opioid receptor (Manglik et al., 2012) structures. Moreover, the same cholesterol, after building the 'rhombic' tetramer hM_3R models, superimposed well with the cholesterol observed in the extracellular side of TMD VII of the $P2Y_{12}$ receptor (Zhang et al, 2014). In addition to such direct observations, Cang et al., (2013) have computationally predicted a cholesterol to be in a similar position in the ß$_2$-adrenoceptor. We, therefore, specifically introduced these cholesterols into the models (**Figure 13**). In such detailed models of the 'rhombic' tetramer (**Figure 13**), molecules of cholesterol bridge the dimer + dimer interface to fill the gap. The model built to describe the experimental mutagenesis results has two cholesterols interacting with TMD VI near the extracellular side which, in the 'rhombic' tetramer constructs, create a layer of four cholesterol molecules that line up to form a buffer between the dimers (**Figure 13**). These mediate interactions of TMD VII with TMD VI as well as with residues from TMD I. This model is consistent with data from the TMD VII mutant, F525A, L528A, L532A, I535A hM_3R. This mutant had a dramatic effect on quaternary structure. Even limiting the alterations to a pair of amino acids (L532A, I535A)(positions 7.41 and 7.44) had an equally dramatic effect. It is noteworthy that McMillin et al., (2011) also reported that a mutation of hM_3R encompassing residues L532A and I535A resulted in substantial disruption of quaternary structure. However, although McMillin and colleagues (2011) suggested, based on these results, a TMD VII-TMD VI

Molecular Pharmacology Fast Forward. Published on March 13, 2015 as DOI: 10.1124/mol.114.096925
This article has not been copyedited and formatted. The final version may differ from this version.

protein-protein contact interface as one possible dimeric arrangement, we offer a very different interpretation that is also consistent with the X-ray structure of M_3R (Kruse et al., 2012). This structure shows that L532A and I535A lie deep in the concave spot of helix TMD VII, a location from which they would be unlikely to form direct residue-residue interactions with TMD VI. However, our model predicts they can do so via the tail of an intermediate molecule of cholesterol (**Figure 13**). This level of structural detail was not available at the time of the report of McMillin et al., (2011). By contrast, limiting the TMD VII mutation to only F525A and L528A generated a receptor variant that was well expressed and displayed no significant deficit in quaternary organization. The 'rhombic' tetramer model also predicts an important role for TMD V. However, rather than at the monomer-monomer interface of the individual dimers, herein the role of TMD V residues is at the dimer + dimer interface. Interestingly, therefore, a clear effect on receptor organization was produced in the TMD V, W252A, R253A hM_3R receptor mutant. The model shows cholesterol binding to the lower part of TMD I and mediating an interaction of TMD I from one dimer with TMD V from the second dimer, specifically involving residues W252 and R253 (**Figure 13**).

Although inherently speculative, the concept that molecules of cholesterol may play integral roles in receptor organization is encouraged from the atomic level structure of the $ß_2$-adrenoceptor (Cherezov et al., 2007). Furthermore, although not a member of the rhodopsin-like family, the dimer of the seven TMD region of the metabotropic glutamate receptor 1 (Wu et al., 2014), shows cholesterol molecules to be situated such that they make an explicit contribution to the receptor-receptor interface. Moreover, Oates et al., (2012) have shown that cholesterol influences activity, stability, and oligomerization of the neurotensin NTS1 receptor.

Molecular Pharmacology Fast Forward. Published on March 13, 2015 as DOI: 10.1124/mol.114.096925
This article has not been copyedited and formatted. The final version may differ from this version.

To generalize this to the analysis of the 'rhombic' tetramer model of the hM_3R is, of course, speculative. Global approaches to sequester cholesterol, for example by the use of agents such as β-methylcyclodextran, are far too crude to assess this proposed key role of cholesterol in a specific manner. Indeed, when we tried to employ β-methylcyclodextran-mediated depletion of cholesterol it was difficult to assess the organization of even the wild type receptor construct (not shown). Despite these challenges, a number of the other mutants that had substantial effects on receptor organization are also compatible with roles for cholesterol. For example, in the TMD I L80A,I83A,I84A,I87A VSV-SNAP-hM_3R mutant, only L80 is predicted to be involved in direct residue-residue interactions in the dimer models we constructed. However, the corresponding residues in these four positions (1.44, 1.47, 1.48 and 1.51) are involved in binding a molecule of cholesterol in both the β_2-adrenoceptor (Cherezov et al., 2007) and the serotonin 5-HT_{2B} (Liu et al., 2013).

It is also intriguing to consider the role of helix VIII in receptor organization. As shown, mutation of the leucine residues at position 8.58 and 8.59 had a large effect on the overall organization of the oligomer. These residues lie next to the cysteine which, in many receptors, defines the end of helix VIII and is palmitoylated in a regulated fashion (Chini and Parenti, 2009). Regulation of palmitoylation may, therefore, play an important role in the stability of receptor structure and organization (Chini and Parenti, 2009, Zheng et al., 2012). As with the bulk of post-translational modifications, this is a feature often eliminated from GPCR constructs employed for crystallization to limit heterogeneity of the protein. Although forming the basis for future work, widespread agreement on contributions of helix VIII to interactions between rhodopsin-family GPCRs (Knepp et al., 2012), makes a contribution of lipid acylation a fascinating possibility.

Molecular Pharmacology Fast Forward. Published on March 13, 2015 as DOI: 10.1124/mol.114.096925
This article has not been copyedited and formatted. The final version may differ from this version.

A clear contribution to organizational structure of residues at the bottom of, but not higher in, TMD IV was also observed, consistent with the results of McMillin et al., (2011). This is not an intrinsic feature that is compatible with the rhombic tetramer model shown in Figure 13. However, it is important to note that Patowary et al., (2013) were unable to discriminate between the 'rhombic tetramer' model and a further higher order complex that might include a hexamer. It is interesting in this regard that some time ago Lopez-Gimenez et al., (2007) developed a 'daisy chain' model of higher oligomers and the positioning of TMD IV in the rhombic tetramer model is at consistent with such a means to extend the oligomer chain.

It is well appreciated that many mutations in GPCRs affect both overall expression levels and the capacity expressed protein to be delivered to the cell surface. As a number of GPCR mutations that are believed to interfere with the effectiveness of homomeric interactions result in the protein being retained within the ER/Golgi apparatus (Salahpour et al., 2004, Lopez-Gimenez et al., 2007, Canals et al., 2009, Kobayashi et al., 2009). It has been suggested on this basis that 'dimerization' of GPCRs is required for cell surface delivery and that effective GPCR dimerization/oligomerization is an integral part of the cellular quality control process. We thus wished to monitor the oligomeric organization only of receptors that had actually reached the cell surface. Traditionally, reporters suitable for resonance energy transfer studies, whether based on BRET or FRET, have been added to the intracellular C-terminal tail of the GPCR being studied (Alvarez-Curto et al., 2010a). However, this results, in BRET studies in particular, being limited to reporting on the total population of expressed receptors, whether at the cell surface or located internally. To overcome this we used a htrFRET-based approach in which the energy donor and acceptor fluorophores were incorporated covalently into a SNAP-tag (Kolberg et al., 2013). This was

Molecular Pharmacology Fast Forward. Published on March 13, 2015 as DOI: 10.1124/mol.114.096925
This article has not been copyedited and formatted. The final version may differ from this version.

introduced into the extracellular N-terminal domain of the receptor. Furthermore, we measured directly both cell surface expression, by taking advantage of the SNAP tag, and the protein expression profile, via immunoblots, to monitor N-glycosylation and protein maturity. These are features routinely linked to effective cell surface delivery (Petaja-Repo and Lackman, 2014). Even for hM_3R mutants that displayed poor cell surface expression, this increased in a linear fashion with increasing amounts of cDNA used to transfect cells. We were able, therefore, to assess receptor-receptor interactions at the cell surface for each mutant compared to the wild type receptor construct at equal levels of cell surface receptor. Most importantly, the slope of the line of energy transfer signal corresponding to receptor-receptor interactions against cell surface expression levels provided a measure of effects of mutations on receptor organizational structure that was independent of effects on expression levels. Systematic use and analysis of this feature provided us with new insights into the most likely quaternary organization.

Pharmacological chaperones have been widely discussed for their potential to treat disorders in which mutations of GPCRs result in intracellular retention and/or poor protein folding (Maya-Nunez et al., 2012, Nakamura et al., 2010). Ligands with such capacity have also been used to rescue, to the cell surface, receptors that have defects in oligomer organization. At least in the context of heterologous expression, even wild type receptors can be chaperoned to the cell surface to increase functional density by the use of ligands able to penetrate the cell and bind to the retained or improperly folded receptor (Leskela et al., 2007). It was interesting, therefore, to note in these studies that sustained treatment of cells expressing various mutants of the hM_3R with the standard muscarinic receptor antagonist/inverse agonist atropine was able to enhance cell surface levels and the N-

Molecular Pharmacology Fast Forward. Published on March 13, 2015 as DOI: 10.1124/mol.114.096925
This article has not been copyedited and formatted. The final version may differ from this version.

glycosylation status of many of the mutants. Most interestingly, atropine treatment generally also resulted in alteration in oligomeric organization of these receptor mutants, with the majority now having organization akin to the wild type receptor. It is further interesting to note in this regard that in FRET-based studies on the organization of the β_2-adrenoceptor reconstituted into a model lipid bilayer Fung et al., (2009) generated results favoring constitutive tetrameric receptor organization. They also observed that addition of an inverse agonist ligand led to tighter packing of protomers and/or the formation of more complex oligomers by reducing conformational fluctuations in individual protomers (Fung et al., 2009). Atropine is a muscarinic blocker that reduces constitutive, basal activity and is, therefore an inverse agonist. It is likely that many receptor mutants that are poorly expressed, contribute to disease, and which have been suggested to be potentially suitable for recovery by treatment with pharmacological chaperones, are actually 'oligomeric organization'-deficient rather than lacking a capacity to bind ligand. As mutations that have such effects are observed in positions throughout receptor protein sequence, the idea that externally facing residues in many helices can contribute to the quaternary organization of a receptor is entirely consistent with both the model and the experimental data.

Overall, these studies provide clear evidence that incorrect organizational structure of many mutants of the hM_3R provides the molecular basis for why they are poorly expressed and fail to be effectively trafficked to the cell surface. They also provide, therefore, further support for models in which dimerization/oligomerization is an integral early step in the cellular recognition and application of protein quality control. Moreover, based on molecular modelling studies that have allowed testable hypotheses, the mutational studies performed herein suggest that a substantial organizational feature of hM_3R, at least when expressed in

Molecular Pharmacology Fast Forward. Published on March 13, 2015 as DOI: 10.1124/mol.114.096925
This article has not been copyedited and formatted. The final version may differ from this version.

such a heterologous system, may be a tetramer with 'rhombic' shape. They also provide insight into the potential contribution of molecules of cholesterol and indeed possibly, regulated palmitoylation, to the overall organization and potential stability of GPCR oligomers. It will be particularly important to develop ways to explore this specific suggested role of cholesterol without the need to generally deplete levels of this lipid. It will also be fascinating to explore whether this model of 'rhombic' organization of receptor tetramers is broadly applicable across the family of rhodopsin-family GPCRs.

Molecular Pharmacology Fast Forward. Published on March 13, 2015 as DOI: 10.1124/mol.114.096925
This article has not been copyedited and formatted. The final version may differ from this version.

Authorship Contributions

Participated in research design; Varela Liste, Caltabiano, Ward, Alvarez-Curto, Marsango, Milligan

Conducted experiments; Varela Liste, Marsango, Ward

Contributed new reagents or analytic tools; Caltabiano, Ward, Alvarez-Curto

Performed data analysis; Varela Liste, Caltabiano, Ward, Alvarez-Curto, Marsango, Milligan

Wrote or contributed to writing of manuscript, Varela Liste, Caltabiano, Ward, Alvarez-Curto, Marsango, Milligan

Molecular Pharmacology Fast Forward. Published on March 13, 2015 as DOI: 10.1124/mol.114.096925
This article has not been copyedited and formatted. The final version may differ from this version.

REFERENCES

Alvarez-Curto E, Pediani JD, and Milligan G (2010a) Applications of fluorescence and bioluminescence resonance energy transfer to drug discovery at G protein coupled receptors. *Anal Bioanal Chem* **398**: 167-180.

Alvarez-Curto E, Ward RJ, Pediani JD, and Milligan G (2010b) Ligand regulation of the quaternary organization of cell surface M3 muscarinic acetylcholine receptors analyzed by fluorescence resonance energy transfer (FRET) imaging and homogeneous time-resolved FRET. *J Biol Chem* **285**: 23318-23330.

Ballesteros JA and Weinstein H (1995) Integrated methods for modelling G-protein coupled receptors. *Methods Neurosci* 366-428.

Canals M, Lopez-Gimenez JF, and Milligan G (2009) Cell surface delivery and structural re-organization by pharmacological chaperones of an oligomerization-defective alpha(1b)-adrenoceptor mutant demonstrates membrane targeting of GPCR oligomers. *Biochem J* **417**: 161-172.

Cang X, Du Y, Mao Y, Wang Y, Yang H, and Jiang H (2013) Mapping the functional binding sites of cholesterol in β2-adrenergic receptor by long-time molecular dynamics simulations. *J Phys Chem B* **117**: 1085-1094.

Cherezov V, Rosenbaum DM, Hanson MA, Rasmussen SG, Thian FS, Kobilka TS, Choi HJ, Kuhn P, Weis WI, Kobilka BK, and Stevens RC (2007) High-resolution crystal structure of an engineered human beta2-adrenergic G protein-coupled receptor. *Science* **318**: 1258-1265.

Molecular Pharmacology Fast Forward. Published on March 13, 2015 as DOI: 10.1124/mol.114.096925
This article has not been copyedited and formatted. The final version may differ from this version.

Chini B, and Parenti M (2009) G-protein-coupled receptors, cholesterol and palmitoylation: facts about fats. *J Mol Endocrinol* **42**: 371-379.

Dunham JH, and Hall RA (2009) Enhancement of the surface expression of G protein-coupled receptors. *Trends Biotechnol* **27**: 541-545.

Ehlert FJ, Pak KJ, and Griffin MT (2012) Muscarinic agonists and antagonists: effects on gastrointestinal function. *Handb Exp Pharmacol* **208**: 343-374.

Ferré S, Casadó V, Devi LA, Filizola M, Jockers R, Lohse MJ, Milligan G, Pin JP, and Guitart X (2014) G protein-coupled receptor oligomerization revisited: functional and pharmacological perspectives. *Pharmacol Rev* **66**: 413-434.

Fung JJ, Deupi X, Pardo L, Yao XJ, Velez-Ruiz GA, Devree BT, Sunahara RK, and Kobilka BK (2009) Ligand-regulated oligomerization of beta(2)-adrenoceptors in a model lipid bilayer. *EMBO J.* **28**, 3315-3328

Goin JC, and Nathanson NM (2006) Quantitative analysis of muscarinic acetylcholine receptor homo- and heterodimerization in live cells: regulation of receptor down-regulation by heterodimerization. *J Biol Chem* **281**: 5416-5425.

Guo W, Shi L, Filizola M, Weinstein H, and Javitch JA (2005) Crosstalk in G protein-coupled receptors: changes at the transmembrane homodimer interface determine activation. *Proc Natl Acad Sci USA* **102**:17495-17500

Hern JA, Baig AH, Mashanov GI, Birdsall B, Corrie JE, Lazareno S, Molloy JE, and Birdsall NJ (2010) Formation and dissociation of M1 muscarinic receptor dimers seen by total internal reflection fluorescence imaging of single molecules. *Proc. Natl. Acad. Sci. U S A* **107**:2693-2698.

Hess B, Kutzner C, van der Spoel D, and Lindahl, E. (2008) GROMACS 4: Algorithms for highly hfficient, load-balanced, and scalable molecular simulation. *J. Chem. Theory Comput.* **4:** 435-447.

Hu J, Thor D, Zhou Y, Liu T, Wang Y, McMillin SM, Mistry R, Challiss RA, Costanzi S, and Wess J (2012) Structural aspects of M_3 muscarinic acetylcholine receptor dimer formation and activation. *FASEB J* **26**: 604-616.

Huang J, Chen S, Zhang JJ, and Huang XY (2013) Crystal structure of oligomeric β1-adrenergic G protein-coupled receptors in ligand-free basal state. *Nat Struct Mol Biol* **20:** 419-425.

Jaakola VP, Griffith MT, Hanson MA, Cherezov V, Chien EY, Lane JR, Ijzerman AP, and Stevens RC (2008) The 2.6 angstrom crystal structure of a human A2A adenosine receptor bound to an antagonist. *Science* **322**: 1211-1217.

Knepp AM, Periole X, Marrink SJ, Sakmar TP, and Huber T (2012) Rhodopsin forms a dimer with cytoplasmic helix 8 contacts in native membranes. *Biochemistry* **51**: 1819-1821.

Kobayashi H, Ogawa K, Yao R, Lichtarge O, and Bouvier M (2009) Functional rescue of beta-adrenoceptor dimerization and trafficking by pharmacological chaperones. *Traffic* **10**: 1019-1033.

Kolberg K, Puettmann C, Pardo A, Fitting J, and Barth S (2013) SNAP-tag technology: a general introduction. *Curr Pharm Des* **19**: 5406-5413.

Kruse AC, Hu J, Pan AC, Arlow DH, Rosenbaum DM, Rosemond E, Green HF, Liu T, Chae PS, Dror RO, Shaw DE, Weis WI, Wess J, and Kobilka BK (2012) Structure and dynamics of the M3 muscarinic acetylcholine receptor. *Nature* **482**: 552-556

Kruse AC, Kobilka BK, Gautam D, Sexton PM, Christopoulos A, and Wess J (2014) Muscarinic acetylcholine receptors: novel opportunities for drug development. *Nat Rev Drug Discov* **13**: 549-560.

Leidenheimer NJ, and Ryder KG (2014) Pharmacological chaperoning: a primer on mechanism and pharmacology. *Pharmacol Res* **83**:10-19.

Leskelä TT, Markkanen PM, Pietilä EM, Tuusa JT, and Petäjä-Repo UE (2007) Opioid receptor pharmacological chaperones act by binding and stabilizing newly synthesized receptors in the endoplasmic reticulum. *J Biol Chem* **282**: 23171-23183.

Liu W, Wacker D, Gati C, Han GW, James D, Wang D, Nelson G, Weierstall U, Katritch V, Barty A, Zatsepin NA, Li D, Messerschmidt M, Boutet S, Williams GJ, Koglin JE, Seibert MM, Wang C, Shah ST, Basu S, Fromme R, Kupitz C, Rendek KN, Grotjohann I, Fromme P, Kirian RA, Beyerlein KR, White TA, Chapman HN, Caffrey M, Spence JC, Stevens RC, and

Cherezov V (2013) Serial femtosecond crystallography of G protein-coupled receptors. *Science* **342**: 1521-1524.

Lohse MJ (2010) Dimerization in GPCR mobility and signaling. *Curr Opin Pharmacol* **10**: 53-58.

Lopez-Gimenez JF, Canals M, Pediani JD, and Milligan G (2007) The alpha1b-adrenoceptor exists as a higher-order oligomer: effective oligomerization is required for receptor maturation, surface delivery, and function. *Mol Pharmacol* **71**: 1015-1029.

McMillin SM, Heusel M, Liu T, Costanzi S, and Wess J (2011) Structural basis of M3 muscarinic receptor dimer/oligomer formation. *J Biol Chem* **286**: 28584-92858.

Ma AW, Redka DS, Pisterzi LF, Angers S, and Wells JW (2007) Recovery of oligomers and cooperativity when monomers of the M2 muscarinic cholinergic receptor are reconstituted into phospholipid vesicles. *Biochemistry* **46**:7907-7927.

Manglik A, Kruse AC, Kobilka TS, Thian FS, Mathiesen JM, Sunahara RK, Pardo L, Weis WI, Kobilka BK, and Granier S (2012) Crystal structure of the μ-opioid receptor bound to a morphinan antagonist. *Nature* **485**:321-326.

Martí-Renom MA, Stuart AC, Fiser A, Sánchez R, Melo F, and Sali A (2000) Comparative protein structure modeling of genes and genomes. *Annu Rev Biophys Biomol Struct* **29**: 291-325.

Maya-Núñez G, Ulloa-Aguirre A, Janovick JA, and Conn PM (2012) Pharmacological chaperones correct misfolded GPCRs and rescue function: protein trafficking as a therapeutic target. *Subcell Biochem* **63**: 263-289.

Milligan G (2000) Neurobiology. Receptors as kissing cousins. *Science* **288**:65-67.

Milligan G (2004) G protein-coupled receptor dimerization: function and ligand pharmacology. *Mol Pharmacol* **66**: 1-7.

Milligan G (2009) G protein-coupled receptor hetero-dimerization: contribution to pharmacology and function. *Br J Pharmacol* **158**: 5-14.

Milligan G (2013) The prevalence, maintenance and relevance of G protein-coupled receptor oligomerization. *Mol Pharmacol* **84**: 158-169.

Nakajima K, Jain S, Ruiz de Azua I, McMillin SM, Rossi M, and Wess J (2013) Minireview: Novel aspects of M3 muscarinic receptor signaling in pancreatic β-cells. *Mol Endocrinol* **27**: 1208-1216.

Nakamura M, Yasuda D, Hirota N, and Shimizu T (2010) Specific ligands as pharmacological chaperones: The transport of misfolded G-protein coupled receptors to the cell surface. *IUBMB Life* **62**: 453-459.

Nenasheva TA, Neary M, Mashanov GI, Birdsall NJ, Breckenridge RA, and Molloy JE (2013) Abundance, distribution, mobility and oligomeric state of M_2 muscarinic acetylcholine receptors in live cardiac muscle. *J Mol Cell Cardiol* **57**:129-136.

Oates J, Faust B, Attrill H, Harding P, Orwick M, and Watts A (2012) The role of cholesterol on the activity and stability of neurotensin receptor 1. *Biochim Biophys Acta* **1818**: 2228-2233.

Park PS. Sum CS, Pawagi AB, and Wells JW (2002) Cooperativity and oligomeric status of cardiac muscarinic cholinergic receptors. *Biochemistry* **41**: 5588-5604.

Patowary S, Alvarez-Curto E, Xu TR, Holz JD, Oliver JA, Milligan G, and Raicu V (2013) The muscarinic M3 acetylcholine receptor exists as two differently sized complexes at the plasma membrane. *Biochem J* **452**: 303-312.

Petäjä-Repo UE, and Lackman JJ (2014).Targeting opioid receptors with pharmacological chaperones. *Pharmacol Res* **83**: 52-62.

Rasmussen SGF, Devree BT, Zou Y, Kruse AC, Chung KY, Kobilka TS, Thian FS, Chae PS, Pardon E, Calinski D, Mathiesen JM, Shah STA, Lyons JA, Caffrey M, Gellman SH, Steyaert J, Skiniotis G, Weis WI, Sunahara RK, and Kobilka BK (2012) Crystal structure of the β2 adrenergic receptor-Gs protein complex. *Nature* **477**: 549–555.

Redka DS, Morizumi T, Elmslie G, Paranthaman P, Shivnaraine RV, Ellis J, Ernst OP, and Wells JW (2014) Coupling of G Proteins to reconstituted monomers and tetramers of the M2 muscarinic receptor. *J Biol Chem* **289**: 24347-24365.

Ruiz de Azua I, Gautam D, Jain S, Guettier JM, and Wess J (2012) Critical metabolic roles of β-cell M3 muscarinic acetylcholine receptors. *Life Sci* **91**: 986-991.

Salahpour A, Angers S, Mercier JF, Lagacé M, Marullo S, and Bouvier M (2004) Homodimerization of the beta2-adrenergic receptor as a prerequisite for cell surface targeting. *J Biol Chem* **279**: 33390-33397.

Schro□dinger LLC (2012) The PyMOL Molecular Graphics System, version 1.5r3, Schro□dinger LLC, Cambridge, MA.

Sumida T, Tsuboi H, Iizuka M, Asashima H, and Matsumoto I (2013) Anti-M3 muscarinic acetylcholine receptor antibodies in patients with Sjögren's syndrome. *Mod Rheumatol* **23**: 841-845.

Wacker D, Wang C, Katritch V, Han GW, Huang XP, Vardy E, McCorvy JD, Jiang Y, Chu M, Siu FY, Liu W, Xu HE, Cherezov V, Roth B., and Stevens RC (2013) Structural features for functional selectivity at serotonin receptors. *Science* **340**: 615-619.

Ward RJ, and Milligan G. (2014) Structural and biophysical characterisation of G protein-coupled receptor ligand binding using resonance energy transfer and fluorescent labelling techniques. *Biochim Biophys Acta* **1838**: 3-14.

Wess J (1996) Molecular biology of muscarinic acetylcholine receptors. *Crit Rev Neurobiol* **10**: 69–99.

Wilson S, Wilkinson G, and Milligan G (2005) The CXCR1 and CXCR2 receptors form constitutive homo- and heterodimers selectively and with equal apparent affinities. *J Biol Chem* **280**: 28663-26874.

Wu H, Wacker D, Mileni M, Katritch V, Han GW, Vardy E, Liu W, Thompson AA, Huang

XP, Carroll FI, Mascarella SW, Westkaemper RB, Mosier PD, Roth BL, Cherezov V, and Stevens RC (2012) Structure of the human κ-opioid receptor in complex with JDTic. *Nature* **485**: 327-332.

Wu H, Wang C, Gregory KJ, Han GW, Cho HP, Xia Y, Niswender CM, Katritch V, Meiler J, Cherezov V, Conn PJ, and Stevens RC (2014) Structure of a class C GPCR metabotropic glutamate receptor 1 bound to an allosteric modulator. *Science* **344**: 58-64.

Xu TR, Ward RJ, Pediani JD, and Milligan G (2012) Intramolecular fluorescence resonance energy transfer (FRET) sensors of the orexin OX1 and OX2 receptors identify slow kinetics of agonist activation. *J Biol Chem* **287**: 14937-14949.

Zhang K, Zhang J, Gao ZG, Zhang D, Zhu L, Han GW, Moss SM, Paoletta S, Kiselev E, Lu W, Fenalti G, Zhang W, Müller CE, Yang H, Jiang H, Cherezov V, Katritch V, Jacobson KA, Stevens RC, Wu B, and Zhao Q (2014) Structure of the human P2Y12 receptor in complex with an antithrombotic drug. *Nature* **509**: 115-118.

Zheng H, Pearsall EA, Hurst DP, Zhang Y, Chu J, Zhou Y, Reggio PH, Loh HH, and Law PY (2012) Palmitoylation and membrane cholesterol stabilize μ-opioid receptor homodimerization and G protein coupling. *BMC Cell Biol* **13**:6.

Molecular Pharmacology Fast Forward. Published on March 13, 2015 as DOI: 10.1124/mol.114.096925
This article has not been copyedited and formatted. The final version may differ from this version.

Molecular Pharmacology Fast Forward. Published on March 13, 2015 as DOI: 10.1124/mol.114.096925
This article has not been copyedited and formatted. The final version may differ from this version.

Footnotes

This work was supported by The Medical Research Council (UK) grants [MR/L023806/1 and G0900050] to GM. MJVL thanks the Fundación Pedro Barrié de la Maza for support, SM thanks the Istituto Pasteur, Fondazione Cenci-Bolognetti for support and GC thanks The European Molecular Biology Organization for a short term Fellowship

Molecular Pharmacology Fast Forward. Published on March 13, 2015 as DOI: 10.1124/mol.114.096925
This article has not been copyedited and formatted. The final version may differ from this version.

FIGURE LEGENDS

Figure 1 At the cell surface VSV-SNAP-hM$_3$R is an N-glycosylated, oligomeric complex

A. Lysates from HEK293T cells transfected with empty vector or with VSV-SNAP-hM$_3$R were resolved by SDS-PAGE with or without pre-treatment with PNGaseF and immuno-blotted with either anti-SNAP antiserum (**upper panel**) or with anti-α-tubulin as a loading control (**lower panel**). **B.** Cells transfected with empty vector or varying amounts of VSV-SNAP-hM$_3$R containing plasmid for 24 h were incubated with the htrFRET energy donor (SNAP-Lumi4Tb, 10 nM). Cell surface binding of this ligand was determined by fluorescent emission at 620 nm after excitation at 337 nm and standardized for cell number. **C.** Cells as in **B** were used to measure the specific binding of single concentration of [^{3}H]-NMS, estimated to occupy greater that 95% of the receptor. **D.** Cell surface oligomeric interactions of VSV-SNAP-hM$_3$R were defined by htrFRET. Optimal concentrations of the SNAP-tag htrFRET energy donor and acceptor were established by incubating cells with a fixed concentration of energy donor (SNAP-Lumi4Tb, 10 nM) and various energy acceptor (SNAP-Red) concentrations. htrFRET measured at 665 nm after excitation at 337 nm reflects proximity between labelled copies of VSV-SNAP-hM$_3$R at the cell surface (**D, circles**). Equivalent experiments were performed on cells expressing the single TMD VSV-SNAP-EGF receptor (**D, squares**) at equal levels of cell surface expression as define by binding and emission at 620 nm of SNAP-Lumi4Tb (**D, insert**, **open bars** = mock transfection, **filled bars** = corresponding receptor). **E.** DDM extracts of lysates from HEK293T cells transfected with empty vector or VSV-SNAP-hM$_3$R were prepared and treated or not with 1% SDS before resolution by Blue Native-PAGE and immuno-blotted with the anti-SNAP antiserum.

Molecular Pharmacology Fast Forward. Published on March 13, 2015 as DOI: 10.1124/mol.114.096925
This article has not been copyedited and formatted. The final version may differ from this version.

F. HEK293T cells were transfected with increasing amounts of VSV-SNAP-hM_3R for 24 h and then incubated with the optimal combination and ratio of SNAP-Lumi4Tb (10 nM) and SNAP-Red (100 nM). The htrFRET signal determined as fluorescent emission at 665 nm was plotted as a function of cell surface SNAP-tagged receptor expression measured by fluorescent emission at 620 nm.

Figure 2 Sequence of VSV-SNAP-hM_3R-based receptor mutants

A schematic representation of the VSV-SNAP-hM_3R construct is shown. This was used as template to generate 19 TMD mutants by alanine substitution. Residues mutated simultaneously are grouped by brackets and indicated by the amino acid one-letter code, the corresponding Ballesteros/Weinstein residue positioning number is also provided. The most highly conserved residue in each TMD is indicated by the corresponding Ballesteros/Weinstein number (X.50) within the cylinders that represent each helix. Residues in grey are those in which mutation resulted in reduced oligomeric interactions.

Figure 3 Determination of the level and pattern of expression of wild type and mutated forms of VSV-SNAP-hM_3R

A. HEK293T cells transfected to express wild type or mutated forms of VSV-SNAP-hM_3R were incubated with 10 nM SNAP-Lumi4Tb and cell surface binding was determined as in Figure 1. Data are means ± S.E.M. of at least three independent experiments. ns, not significant, one way ANOVA compared with VSV-SNAP-hM_3R. All other samples were expressed at significantly lower levels than VSV-SNAP-hM_3R.

Molecular Pharmacology Fast Forward. Published on March 13, 2015 as DOI: 10.1124/mol.114.096925
This article has not been copyedited and formatted. The final version may differ from this version.

B, C. Cell lysates prepared from HEK293T cells transfected with the above constructs were resolved by SDS-PAGE and immuno-blotted with anti-SNAP antiserum. Immunoblotting of the same samples with an anti-α-tubulin antiserum is also shown as a loading control.

Figure 4 Many regions of the helical domains of hM_3R contribute to effective oligomerization

htrFRET experiments for each mutant studied, including those shown in Figures 5-9, were analysed by linear regression. The slope values of 665 nm over 620 nm fluorescence emission as defined in Figures 5-9 were then normalized relative to the slope value obtained with VSV-SNAP-hM_3R (which was included as control in each individual experiment). Data are means ± S.E.M. of at least three independent experiments. ***, $p < 0.001$ and * $p < 0.05$, one way ANOVA compared with VSV-SNAP-hM_3R.

Figure 5 Mutation of residues at the intracellular end of TMD V of hM_3R alters both expression and oligomeric interactions

A. Representation of the primary sequence of TMD V from hM_3R indicated by the one-letter amino acid code with residue numbering of amino acids that were replaced with alanine shown with dark background and position in the primary sequence of hM_3R. Proline residue 5.50 is also highlighted. The residues mutated are shown as sticks in the cartoon representation of hM_3R. **B.** Representative htrFRET assays performed in HEK293T cells transfected with differing amounts of VSV-SNAP- hM_3R (circles), W252A,R253A VSV-SNAP-hM_3 R (squares) or W252A,R253A,Y255A VSV- SNAP- hM_3R (triangles).

Molecular Pharmacology Fast Forward. Published on March 13, 2015 as DOI: 10.1124/mol.114.096925
This article has not been copyedited and formatted. The final version may differ from this version.

Following incubation with a combination of SNAP-Lumi4Tb (10 nM) and SNAP-Red (100 nM) both fluorescence emission at 620 nm and htrFRET signal (fluorescence emission at 665 nm) were measured. The plot shown was analysed by linear regression.

Figure 6 TMD VI and TMD VII both contribute to the organization of hM_3R receptor oligomers

A. Upper: Representation of the primary sequence of TMD VI from hM_3R indicated by the one-letter amino acid code with residue numbering of amino acids that were replaced with alanine shown with dark background and position in the primary sequence of hM_3R. Proline residue 6.50 is also in bold. **A. Lower:** htrFRET assays akin to those shown in Figure 5 were performed in HEK293T cells transfected with increasing amounts of VSV-SNAP-hM_3R (circles), I502A,I509A VSV-SNAP-hM_3R (squares), V513A,F516A VSV-SNAP-hM_3R (triangles) or I502A,I509A,V513A,F516A VSV-SNAP-hM_3R (open circles) following incubation with a mixture of SNAP-Lumi4Tb (10 nM) and SNAP-Red (100 nM). The data shown were analysed by linear regression.

B. Representation of TMD VII from hM_3R with amino acids represented by the one-letter code and position in the primary sequence. HtrFRET assays were performed as in **A** in cells transfected with increasing amounts of VSV-SNAP-hM_3R (circles), F525A,L528A VSV-SNAP-hM_3 (squares), L532A,I535A VSV-SNAP-hM_3R (triangles) or F525A,L528A,L532A,I535A VSV-SNAP-hM_3R (open circles). Incubation conditions and analysis were as described in Figure 5.

Molecular Pharmacology Fast Forward. Published on March 13, 2015 as DOI: 10.1124/mol.114.096925
This article has not been copyedited and formatted. The final version may differ from this version.

Figure 7 htrFRET studies with TMD I VSV-SNAP-hM$_3$R mutants

A, B, C and D. Upper: Representation of the primary structure of the hM$_3$R TMD I sequence with residues replaced with alanines shown with dark background and indicated by the one-letter amino acid code and number. Asn 1.50 is also shown. **A, B, C and D. Lower:** HtrFRET assays were performed in HEK293T cells transfected with increased amounts of (**A**) the VSV-SNAP-hM$_3$R construct (circles), or Q67A,V68A,I71A,L74A VSV-SNAP-hM$_3$R (triangles); (**B**) VSV-SNAP-hM$_3$R (circles), V69A,F73A VSV-SNAP-hM$_3$R (squares), I77A,L80A VSV-SNAP-hM$_3$R (triangles), V69A,F73A,I77A,L80A VSV-SNAP-hM$_3$R (open circles); (**C**) VSV-SNAP-hM$_3$R (circles) or L80A,I83A,I84A,I87A VSV-SNAP-hM$_3$R (triangles) (**D**) VSV-SNAP-hM$_3$R (circles) or F73A,L80A VSV-SNAP-hM$_3$R (triangles). Incubation conditions and analysis were as described in Figure 5.

Figure 8 Residues at the intracellular end of TMD IV provide protein-protein interactions

A, B. Upper: Representation of the primary sequence of TMD IV from hM$_3$R indicated by the one-letter amino acid code with residue numbering of amino acids that were replaced with alanine shown with dark background and position in the primary sequence of hM$_3$R. Tryptophan residue 4.50 is also in bold. **A. Lower:** htrFRET assays akin to those shown in Figure 5 were performed in HEK293T cells transfected with increasing amounts of VSV-SNAP-hM$_3$R (circles) or L191A,V194A,I195A,V198A VSV-SNAP-hM$_3$R (triangles). **B. Lower:** Experiments as in A used increasing amounts of VSV-SNAP-hM$_3$R (circles) or

Molecular Pharmacology Fast Forward. Published on March 13, 2015 as DOI: 10.1124/mol.114.096925
This article has not been copyedited and formatted. The final version may differ from this version.

K183A,R184A,V187A VSV-SNAP-hM_3R (squares). The data shown were analysed by linear regression.

Figure 9 Intracellular helix VIII also contributes to the oligomeric organization of hM_3R

A. Upper: Representation of the primary structure of helix VIII of the hM_3R sequence with residues replaced with alanines shown on a dark background. Phenylalanine 8.50 is also highlighted. **A. Lower:** Residues altered to alanine for analysis are shown as sticks in the cartoon representation. **B.** Representative htrFRET assay performed on HEK293T cells transfected with increased amounts of the VSV-SNAP-hM_3R construct (circles), or L559A, L560A VSV-SNAP-hM_3R (triangles). Incubation conditions and analysis were as described in Figure 5.**C.** Representative htrFRET assay performed on HEK293T cells transfected with increased amounts of the VSV-SNAP-hM_3R construct (circles), or F555A,K556A,M557A VSV-SNAP-hM_3R (triangles). Incubation conditions and analysis were as described in Figure 5.

Figure 10 Atropine acts as a pharmacological chaperone for many mutants of hM_3R

A.HEK293T cells were transfected to express wild type VSV-SNAP-hM_3R, L80A,I83A,I84A,I87A VSV-SNAP-hM_3R or W252A,R253A VSV-SNAP-hM_3R. The fluorescence emission signal at 620 nm following overnight treatment with either atropine (10 μM) (filled columns) or vehicle (open columns) was measured after incubation of the

Molecular Pharmacology Fast Forward. Published on March 13, 2015 as DOI: 10.1124/mol.114.096925
This article has not been copyedited and formatted. The final version may differ from this version.

cells with 10 nM SNAP-Lumi4Tb and standardized for cell number. * $p < 0.05$, ** $p < 0.01$ Student's t-test compared with the untreated samples. **B**. htrFRET experiments were performed on cells transfected with varying amounts of plasmid encoding either wild type VSV-SNAP-hM_3R (circles) or L80A,I83A,I84A,I87A VSV-SNAP-hM_3R (squares) and maintained in the absence (open symbols) or presence (closed symbols) of atropine (10 μM) for 24h.

Figure 11 Effects of atropine on the organizational structure and N-glycosylation of hM_3R mutants

A. The effect of sustained treatment of cells expressing wild type VSV-SNAP-hM_3R or each of the noted mutants of VSV-SNAP-hM_3R with atropine (10 μM, 24 h) (filled columns) on the oligomeric organization of cell surface-delivered receptor is compared to equivalent cells treated with vehicle (open columns). Data represent the slope of the 665 nm hrtFRET signal versus 620 nm emission signal with cells expressing wild type VSV-SNAP-hM_3R treated with vehicle defined as 1.0. ns, not significant, *** $p < 0.001$, **** $p < 0.0001$ Student's t-test compared with the untreated samples. **B.** Lysates from cells expressing wild type VSV-SNAP-hM_3R or the noted mutants and treated with atropine or vehicle as in **A** were resolved by SDS-PAGE and immunoblotted with an anti-SNAP antiserum (upper section) or an anti-α-tubulin antiserum (lower section)

Figure 12 Molecular models of alternative hM_3R oligomeric arrangements

Molecular Pharmacology Fast Forward. Published on March 13, 2015 as DOI: 10.1124/mol.114.096925
This article has not been copyedited and formatted. The final version may differ from this version.

The figure illustrates three distinct, speculative but conceptually possible, oligomeric molecular models of a hM_3R tetramer: 'rhombic' (**A**) 'linear' (**B**), and 'square' (**C**).

Figure 13 Molecular model of hM_3R oligomeric arrangement based on the experimental results

Centre: model of an hM_3R tetramer with 'rhombic' arrangement as a complex of two dimers (dimeric interface: TMD I-TMD II-helix VIII). Each dimer is shown as a surface. Predicted cholesterols are shown as yellow spheres, four of which create a buffer between the two dimers. **A, B, C, D** and **E** indicate the location of the detailed views shown in the corresponding panels. **A**. Details of TMD I-helix VIII dimer interface. Grey sticks show residues in the cytosolic side of TMD I and in helix VIII. Yellow sticks show cholesterols as observed in crystal structures of the $ß_2$-adrenoceptor and serotonin 5-HT_{2B} receptors. **B**. Predicted interaction on the extracellular side of TMD I-TMD I. F1.37 forms a steric clash with the same residue of the other protomer, while I1.41 and L1.44 create a hydrophobic patch. **C.** Predicted interaction between TMD I of one dimer with TMD V of the other dimer, mediated by a cholesterol molecule (yellow sticks). Grey and light blue sticks represent altered residues of TMD I and TMD V, respectively. The predicted position of the palmitoyl chain bound to Cys 8.60 is also shown (PAM). **D**. Residues (grey sticks) on the extracellular side of TMD I where mutation was found to reduce hrtFRET, possibly interacting with cholesterol. **E.** Possible interface between dimers mediated by cholesterols (yellow sticks) and involving TMD VI from one dimer and TMD VII from the second dimer. Grey and light blue sticks show residues found to be important in this interaction (those buried most deeply in the membrane are shown as spheres).

FIGURE 1

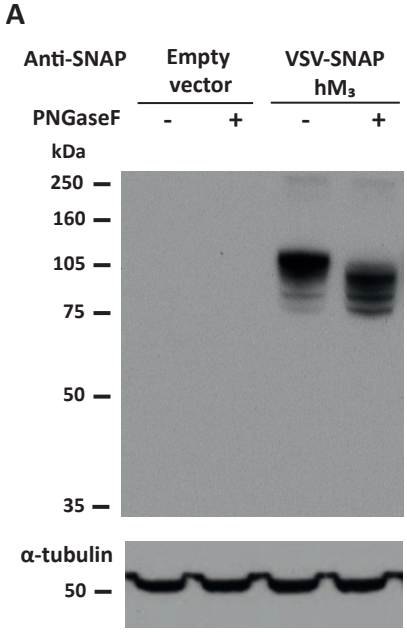
A
Anti-SNAP
Empty vector
VSV-SNAP hM3
PNGaseF
- + - +
kDa
250
160
105
75
50
35
α-tubulin
50

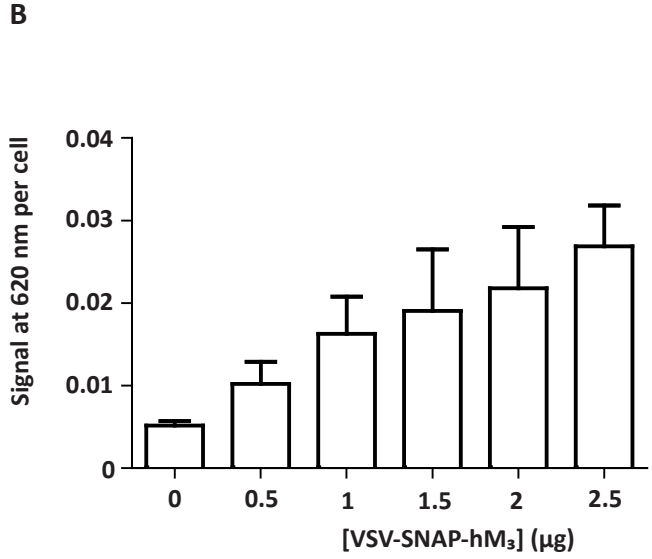
B
Signal at 620 nm per cell
0.04
0.03
0.02
0.01
0
0 0.5 1 1.5 2 2.5
[VSV-SNAP-hM3] (μg)

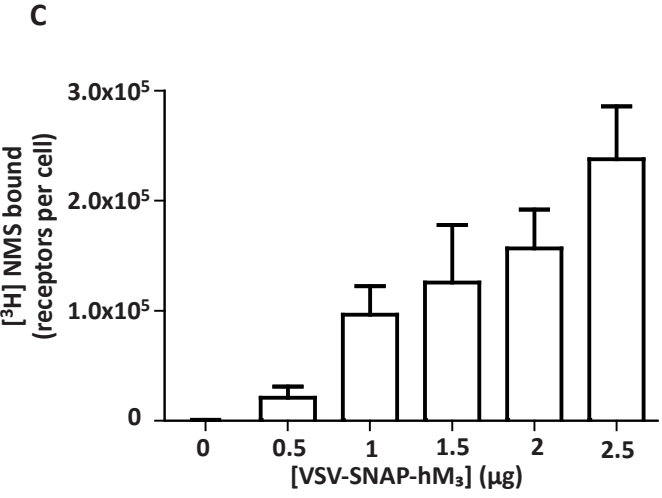
C
[3H] NMS bound (receptors per cell)
3.0x10^5
2.0x10^5
1.0x10^5
0
0 0.5 1 1.5 2 2.5
[VSV-SNAP-hM3] (μg)

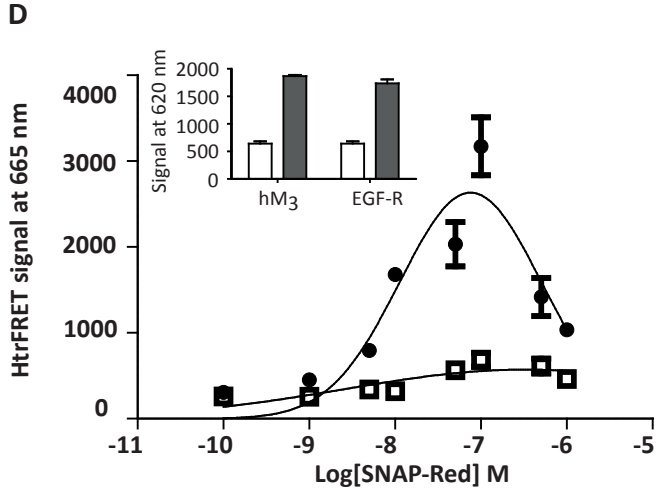
D
HtrFRET signal at 665 nm
4000
3000
2000
1000
0
-11 -10 -9 -8 -7 -6 -5
Log[SNAP-Red] M
Signal at 620 nm
2000
1500
1000
500
0
hM3
EGF-R

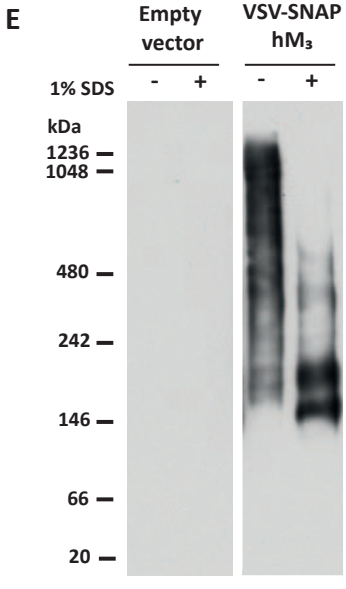
E
Empty vector
VSV-SNAP hM3
1% SDS
- + - +
kDa
1236
1048
480
242
146
66
20

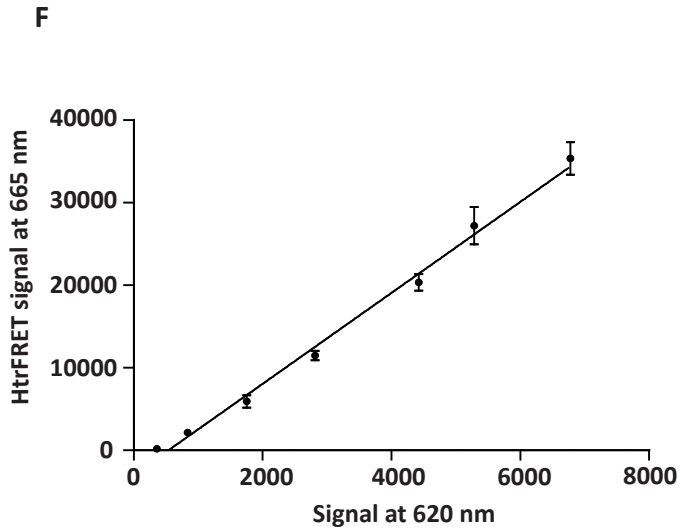
F
HtrFRET signal at 665 nm
40000
30000
20000
10000
0
0 2000 4000 6000 8000
Signal at 620 nm

Molecular Pharmacology Fast Forward. Published on March 13, 2015 as DOI: 10.1124/mol.114.096925
This article has not been copyedited and formatted. The final version may differ from this version.

FIGURE 2

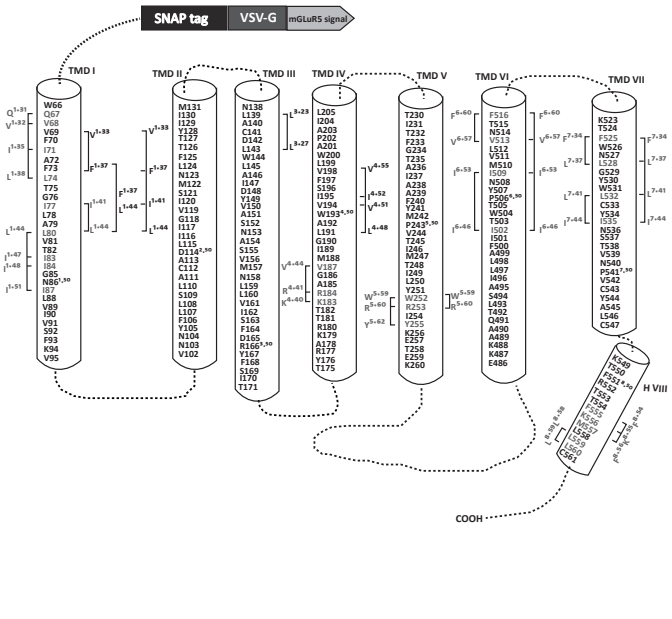

FIGURE 3

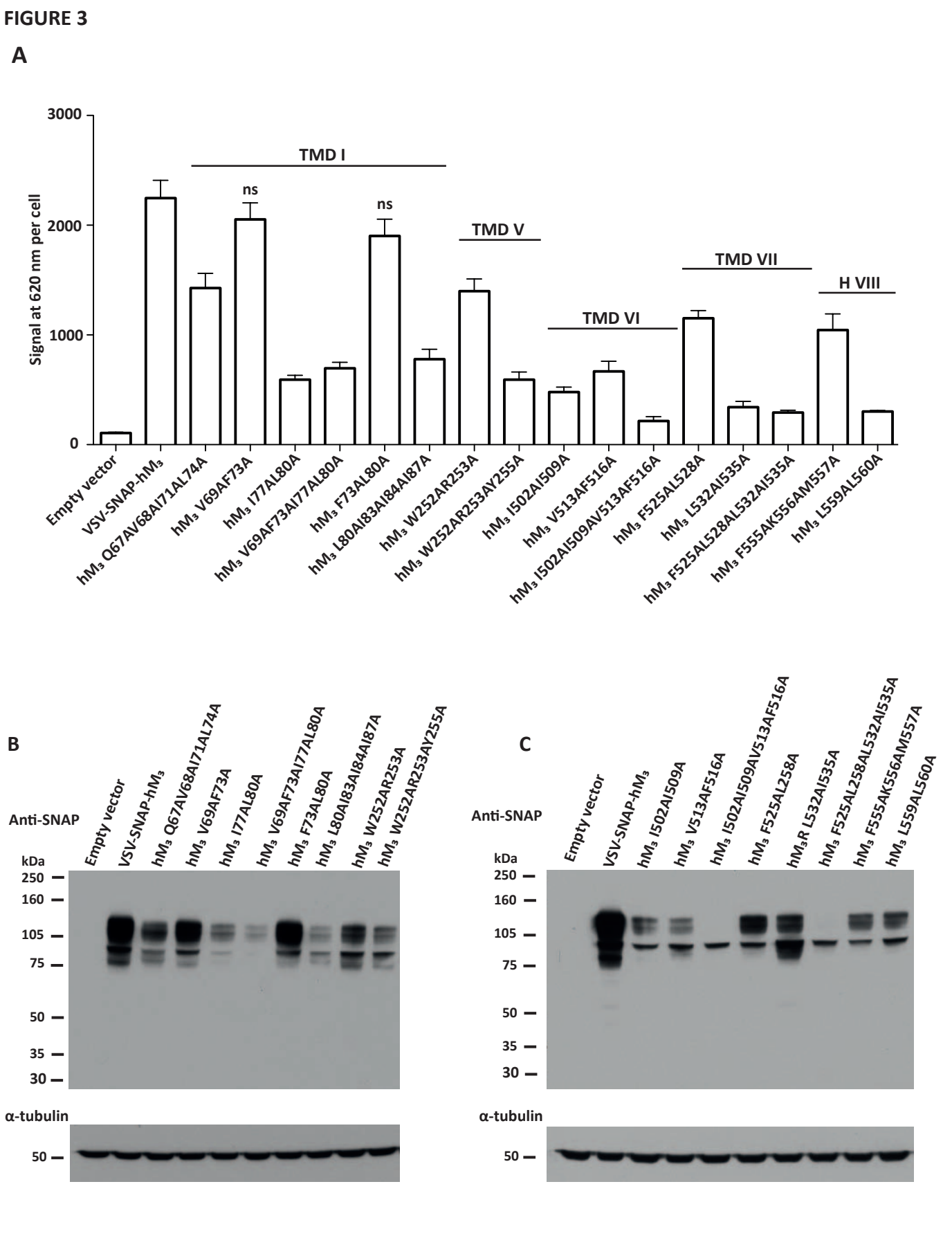
A
3000
2000
1000
0
Signal at 620 nm per cell
TMD I
TMD V
TMD VI
TMD VII
H VIII
ns
ns
Empty vector
VSV-SNAP-hM3
hM3 Q67AV68AI71AL74A
hM3 V69AF73A
hM3 I77AL80A
hM3 V69AF73AI77AL80A
hM3 F73AL80A
hM3 L80AI83AI84AI87A
hM3 W252AR253A
hM3 W252AR253AY255A
hM3 I502AI509A
hM3 V513AF516A
hM3 I502AI509AV513AF516A
hM3 F525AL528A
hM3 L532AI535A
hM3 F525AL528AL532AI535A
hM3 F555AK556AM557A
hM3 L559AL560A
B
Anti-SNAP
kDa
250
160
105
75
50
35
30
α-tubulin
50
C
Anti-SNAP
kDa
250
160
105
75
50
35
30
α-tubulin
50

FIGURE 4

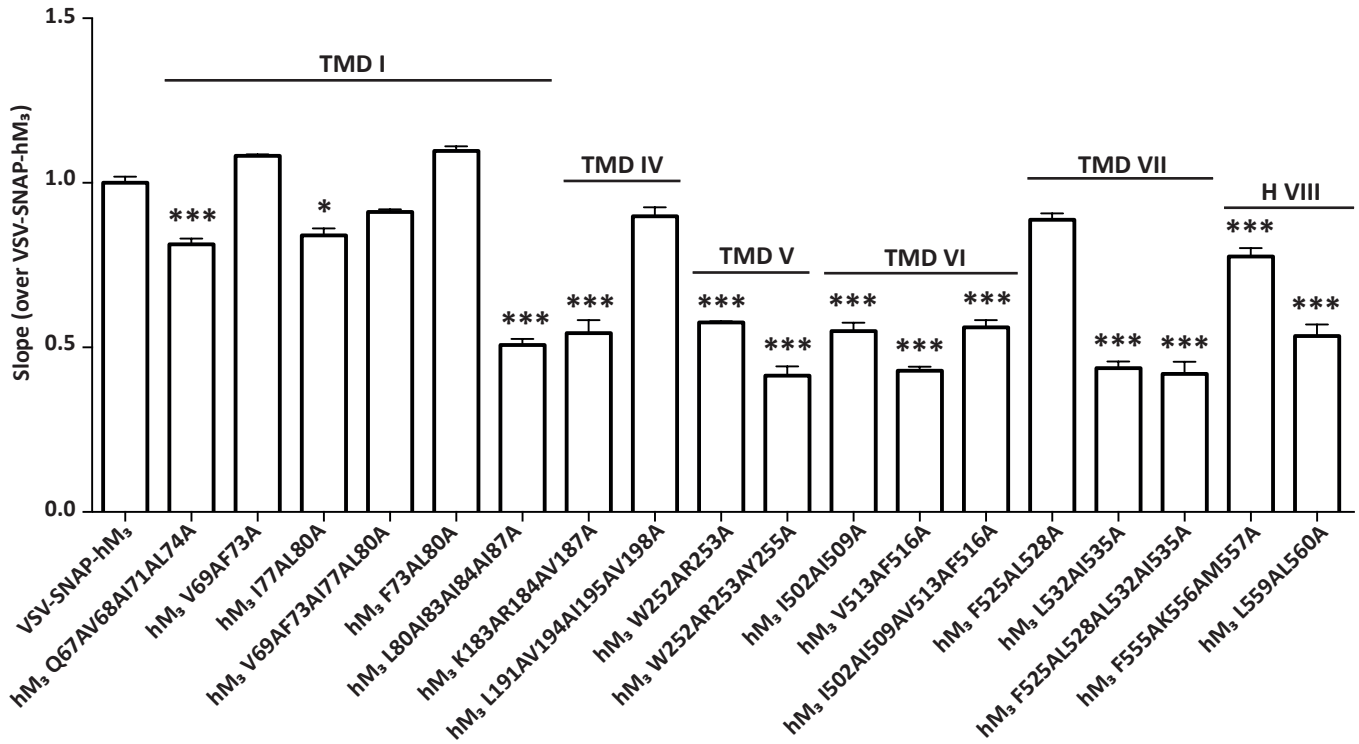
1.5
1.0
0.5
0.0
Slope (over VSV-SNAP-hM3)
TMD I
TMD IV
TMD V
TMD VI
TMD VII
H VIII
***
*
VSV-SNAP-hM3
hM3 Q67AV68AI71AL74A
hM3 V69AF73A
hM3 I77AL80A
hM3 V69AF73AI77AL80A
hM3 F73AL80A
hM3 L80AI83AI84AI87A
hM3 K183AR184AV187A
hM3 L191AV194AI195AV198A
hM3 W252AR253A
hM3 W252AR253AY255A
hM3 I502AI509A
hM3 V513AF516A
hM3 I502AI509AV513AF516A
hM3 F525AL528A
hM3 L532AI535A
hM3 F525AL528AL532AI535A
hM3 F555AK556AM557A
hM3 L559AL560A

FIGURE 5

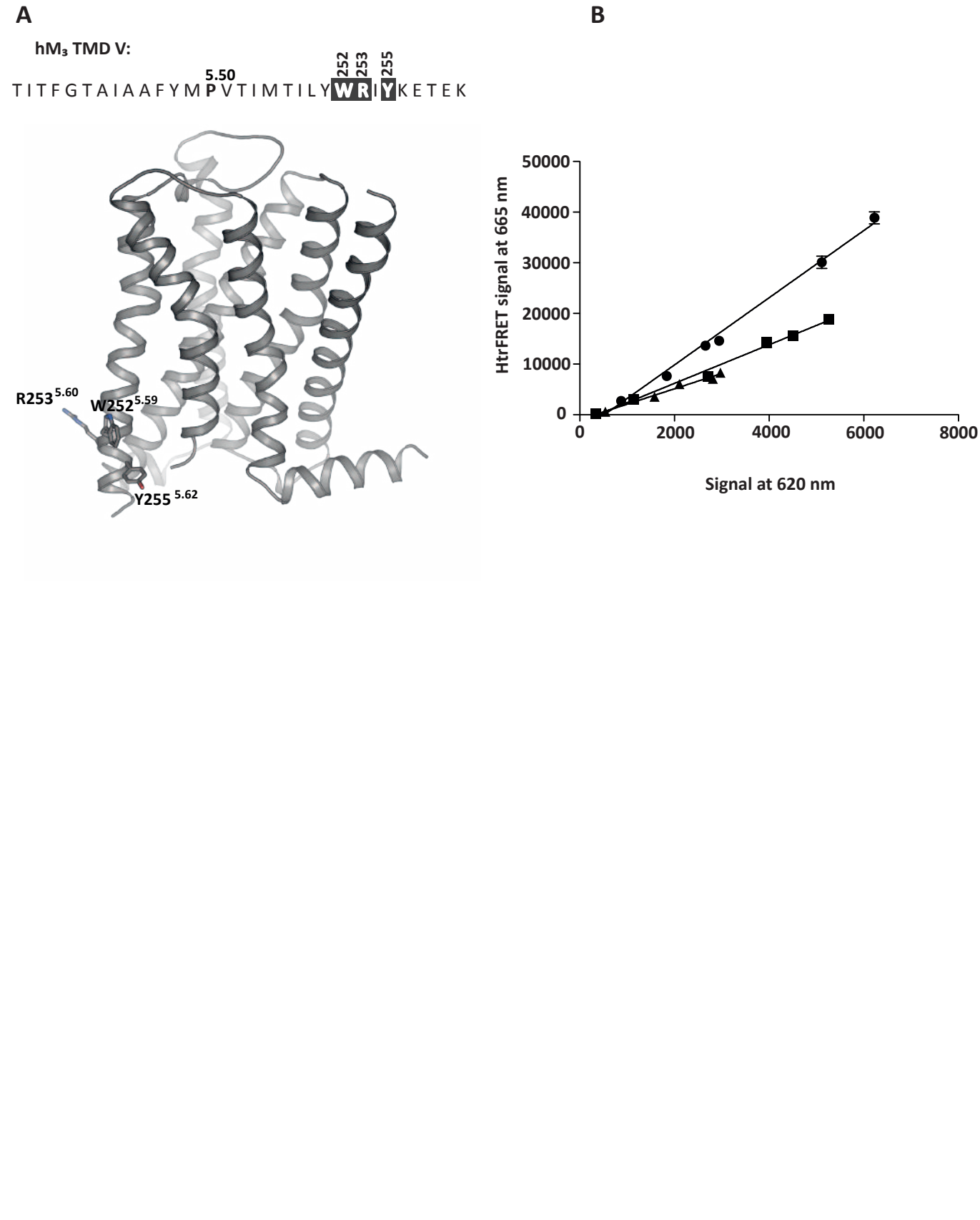
A
hM3 TMD V:
5.50
252
253
255
T I T F G T A I A A F Y M P V T I M T I L Y W R I Y K E T E K
R253 5.60
W252 5.59
Y255 5.62
B
HtrFRET signal at 665 nm
50000
40000
30000
20000
10000
0
0
2000
4000
6000
8000
Signal at 620 nm

FIGURE 6

A

hM_3 TMD VI:

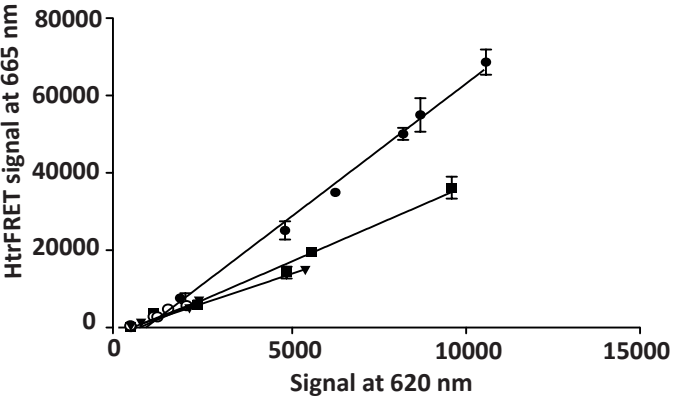

B

hM_3 TMD VII:

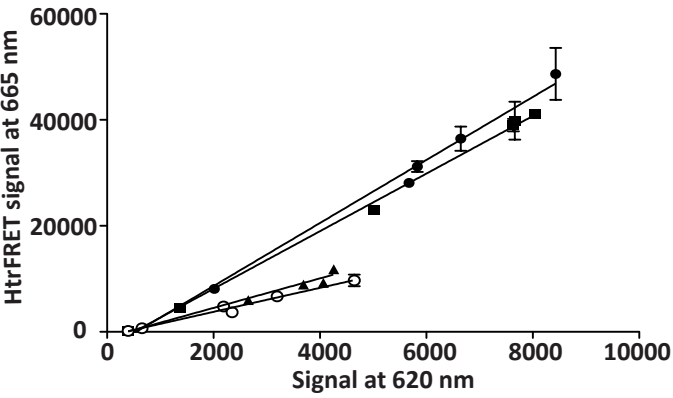

FIGURE 7

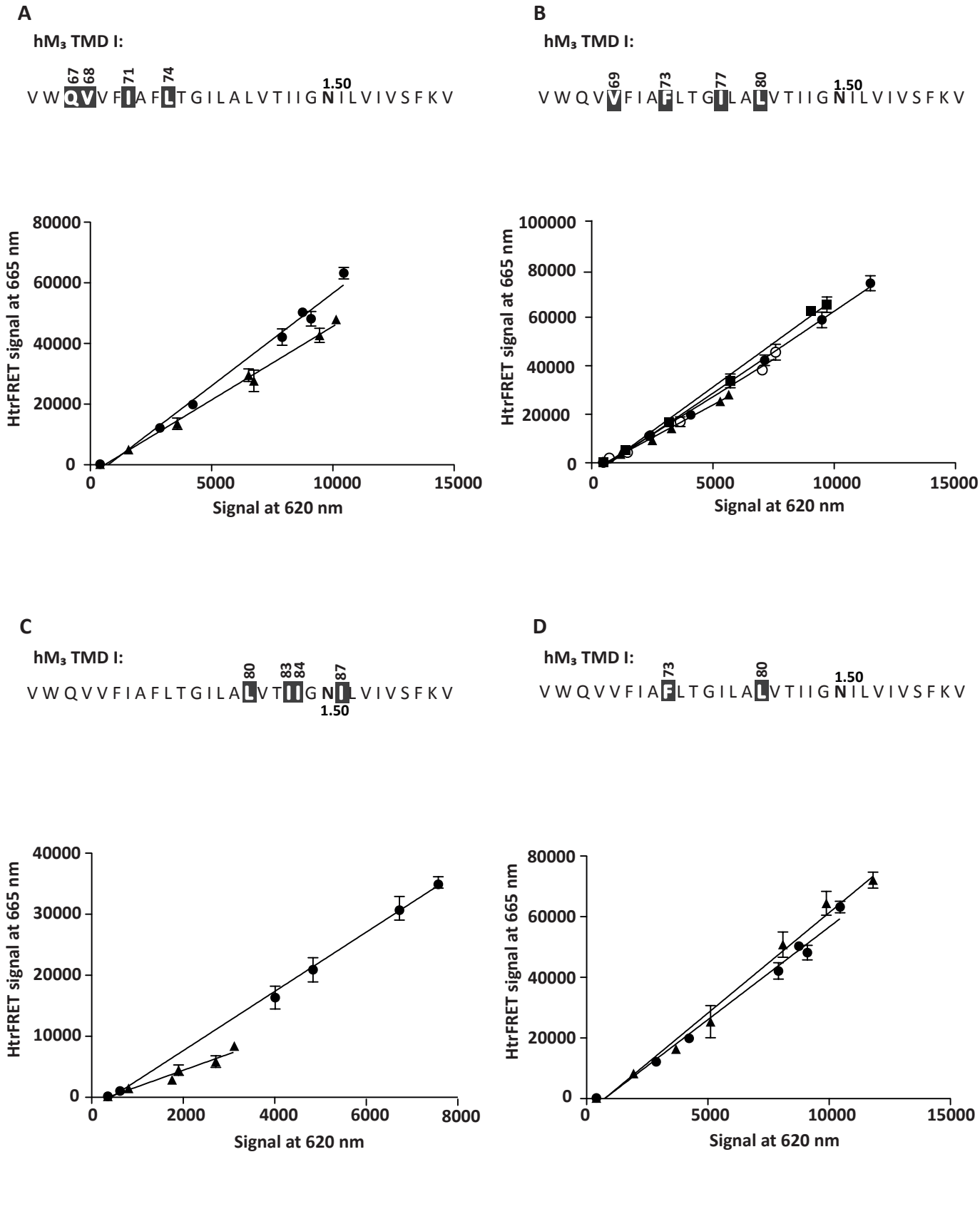
A
hM3 TMD I:
67 68 71 74 1.50
V W Q V V F I A F L T G I L A L V T I I G N I L V I V S F K V
HtrFRET signal at 665 nm
Signal at 620 nm
B
hM3 TMD I:
69 73 77 80 1.50
V W Q V V F I A F L T G I L A L V T I I G N I L V I V S F K V
HtrFRET signal at 665 nm
Signal at 620 nm
C
hM3 TMD I:
80 83 84 87 1.50
V W Q V V F I A F L T G I L A L V T I I G N I L V I V S F K V
HtrFRET signal at 665 nm
Signal at 620 nm
D
hM3 TMD I:
73 80 1.50
V W Q V V F I A F L T G I L A L V T I I G N I L V I V S F K V
HtrFRET signal at 665 nm
Signal at 620 nm

FIGURE 8

A

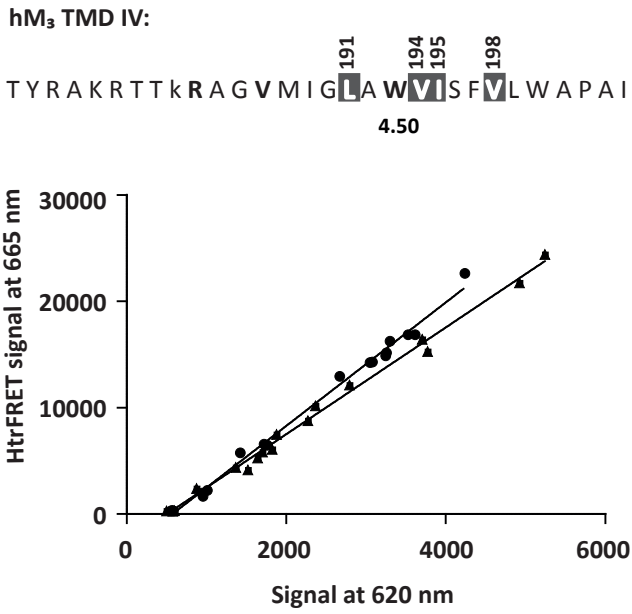
hM₃ TMD IV:
191
194
195
198
TYRAKRTTkRAGVMIGLAWVISFVLWAPAIL
4.50
HtrFRET signal at 665 nm
30000
20000
10000
0
0
2000
4000
6000
Signal at 620 nm

B

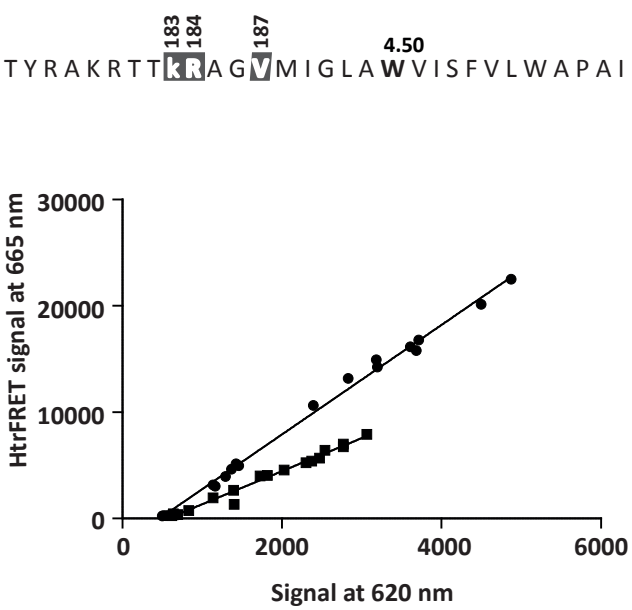
hM₃ TMD IV:
183
184
187
4.50
TYRAKRTTkRAGVMIGLAWVISFVLWAPAIL
HtrFRET signal at 665 nm
30000
20000
10000
0
0
2000
4000
6000
Signal at 620 nm

FIGURE 9

A

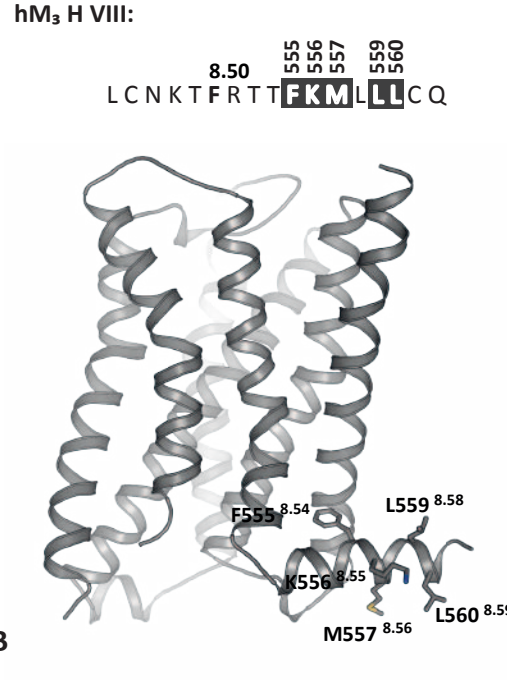
hM3 H VIII:
8.50
555
556
557
559
560
L C N K T F R T T F K M L L C Q
F555 8.54
L559 8.58
K556 8.55
L560 8.59
M557 8.56

B

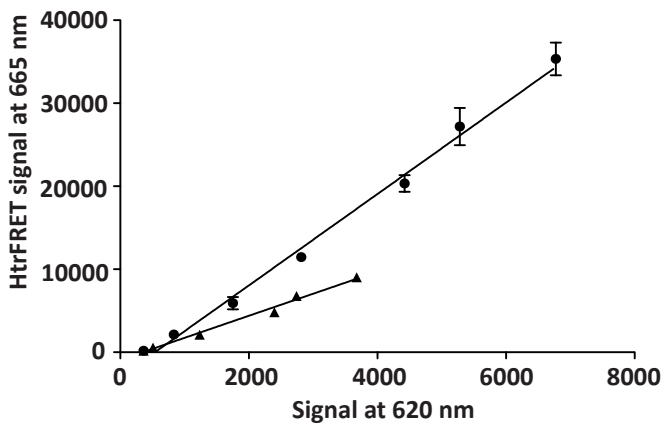
HtrFRET signal at 665 nm
40000
30000
20000
10000
0
0
2000
4000
6000
8000
Signal at 620 nm

C

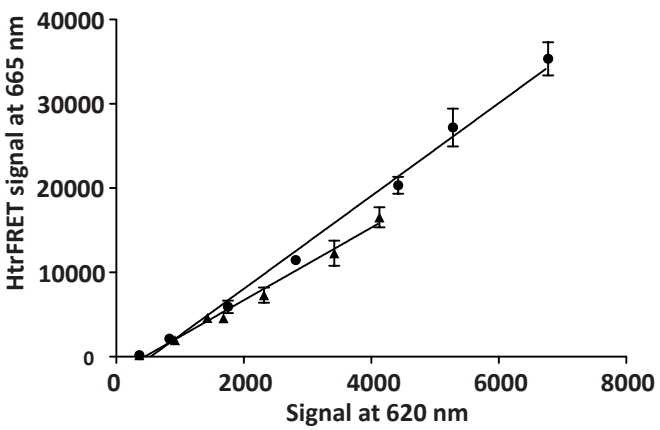
HtrFRET signal at 665 nm
40000
30000
20000
10000
0
0
2000
4000
6000
8000
Signal at 620 nm

FIGURE 10

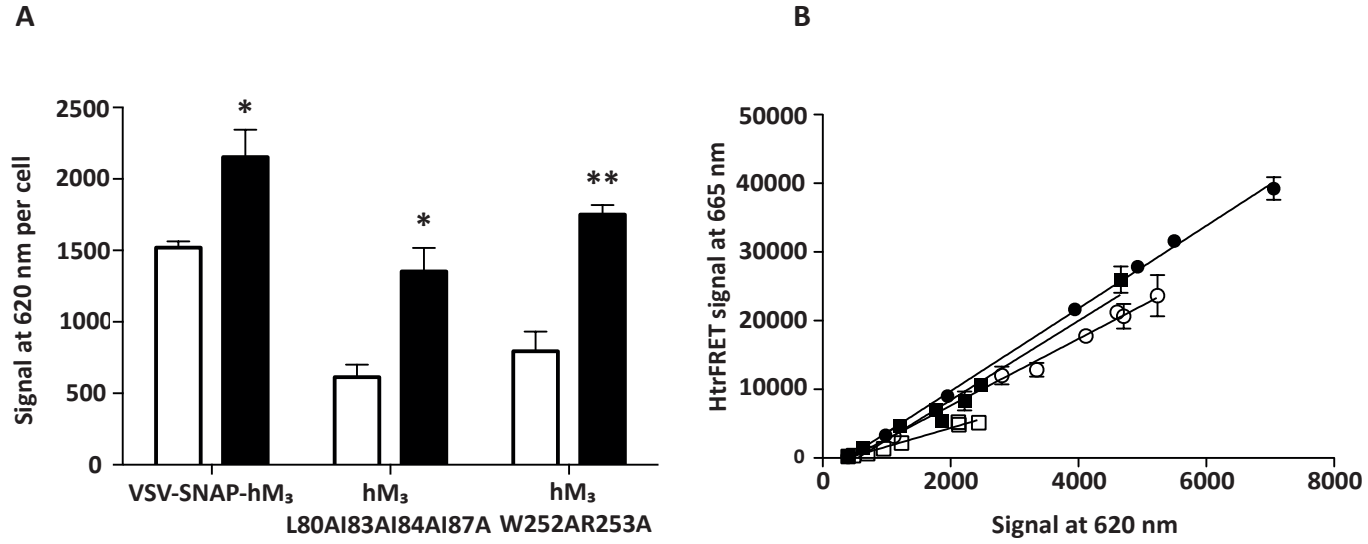
A
B
2500
2000
1500
1000
500
0
Signal at 620 nm per cell
*
*
**
VSV-SNAP-hM₃
hM₃
L80AI83AI84AI87A
hM₃
W252AR253A
50000
40000
30000
20000
10000
0
HtrFRET signal at 665 nm
0
2000
4000
6000
8000
Signal at 620 nm

FIGURE 11

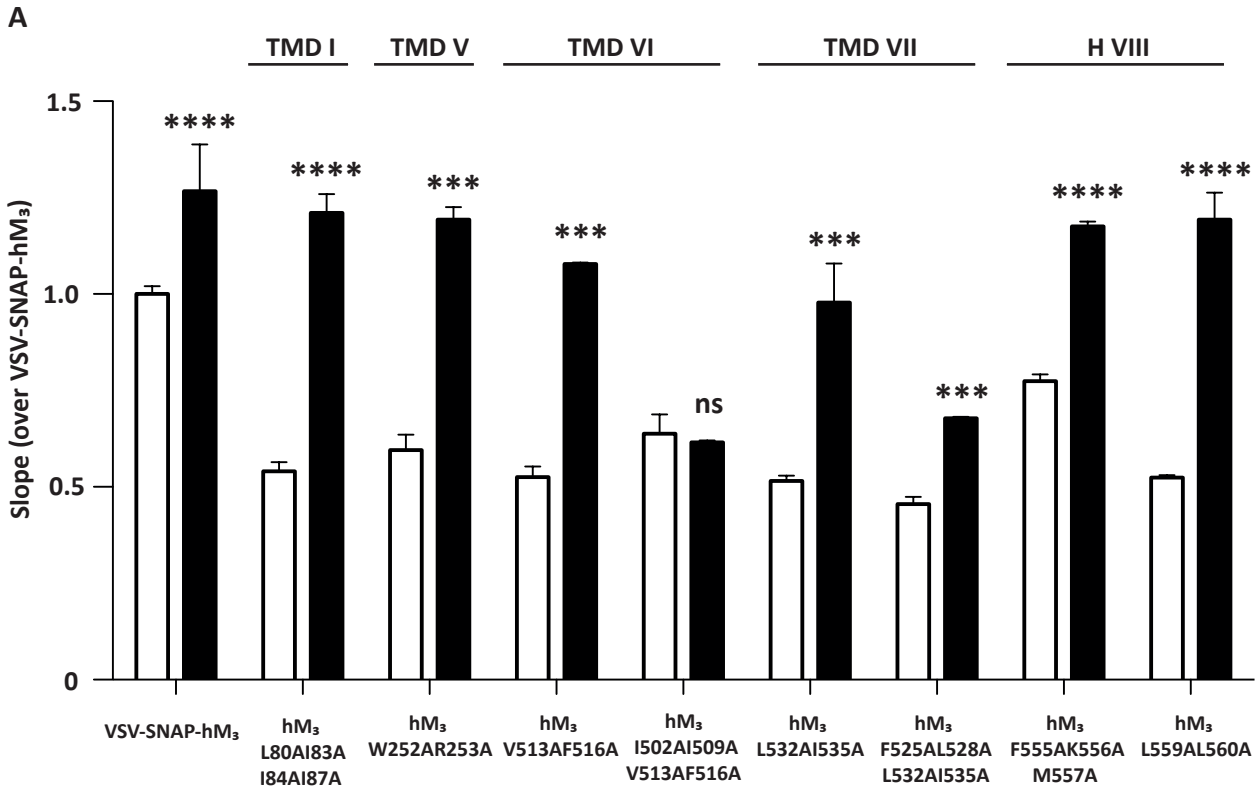
A
TMD I
TMD V
TMD VI
TMD VII
H VIII
Slope (over VSV-SNAP-hM3)
1.5
1.0
0.5
0
****
****
***
***
ns
***
***
****
****
VSV-SNAP-hM3
hM3 L80AI83A I84AI87A
hM3 W252AR253A
hM3 V513AF516A
hM3 I502AI509A V513AF516A
hM3 L532AI535A
hM3 F525AL528A L532AI535A
hM3 F555AK556A M557A
hM3 L559AL560A

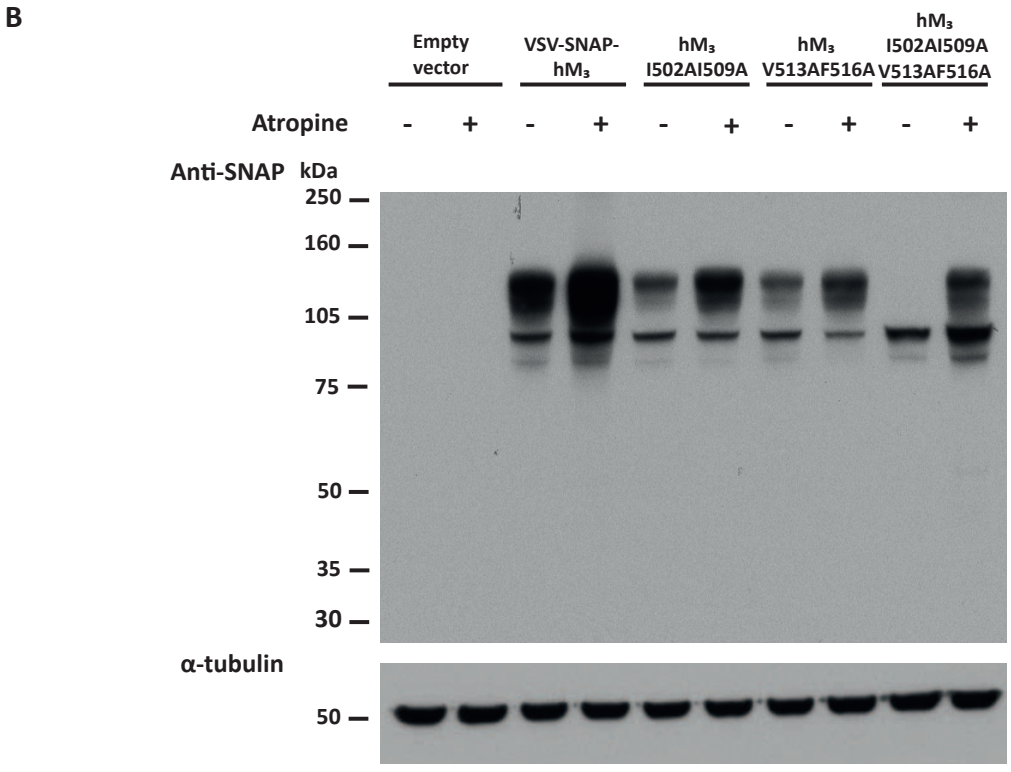
B
Empty vector
VSV-SNAP-hM3
hM3 I502AI509A
hM3 V513AF516A
hM3 I502AI509A V513AF516A
Atropine
- + - + - + - + - +
Anti-SNAP
kDa
250
160
105
75
50
35
30
α-tubulin
50

Figure 12

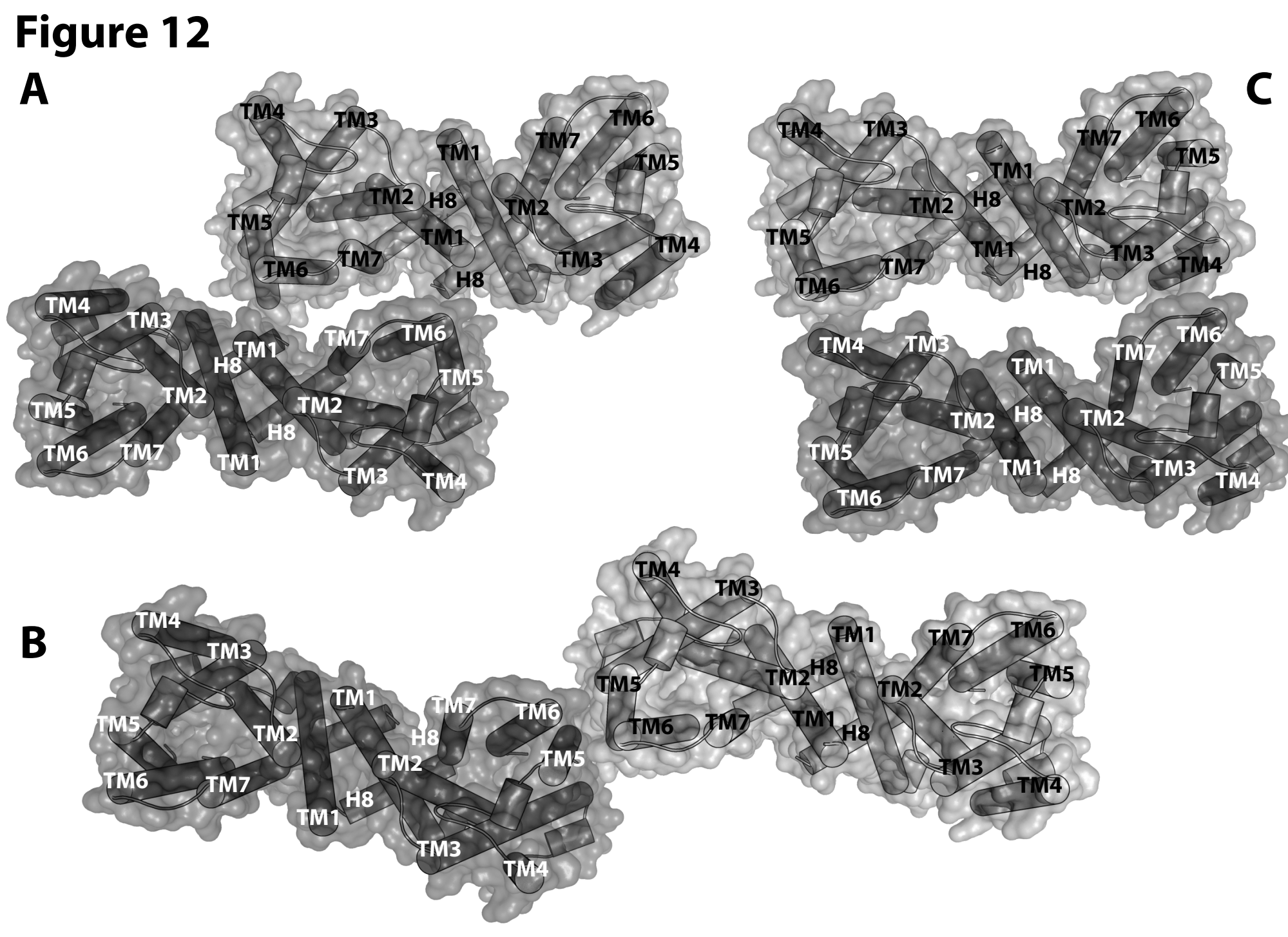
A
TM4
TM3
TM1
TM7
TM6
TM5
TM2
H8
TM5
TM1
TM6
TM7
TM2
TM3
TM4
H8
TM4
TM3
TM1
TM7
TM6
H8
TM5
TM2
TM5
TM2
H8
TM6
TM7
TM1
TM3
TM4
C
TM4
TM3
TM1
TM7
TM6
TM5
TM2
H8
TM5
TM2
TM1
TM6
TM7
H8
TM3
TM4
TM4
TM3
TM1
TM7
TM6
TM5
TM2
H8
TM2
TM5
TM6
TM7
TM1
H8
TM3
TM4
B
TM4
TM3
TM1
TM7
TM6
TM5
TM2
H8
TM5
TM2
TM6
TM7
TM1
H8
TM3
TM4
TM4
TM3
TM1
TM7
TM6
TM5
TM2
H8
TM5
TM2
TM6
TM7
H8
TM1
TM3
TM4

Figure 13

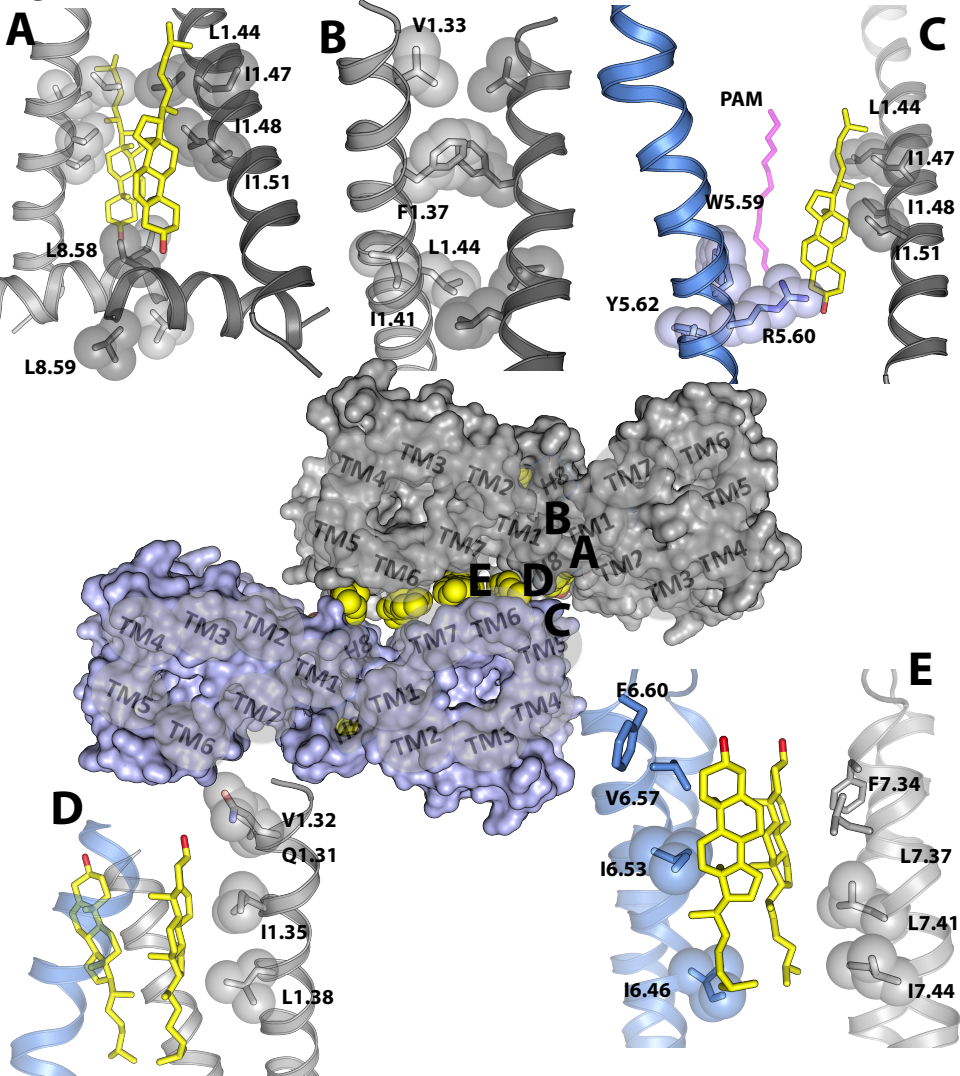
A
L1.44
I1.47
I1.48
I1.51
L8.58
L8.59
B
V1.33
F1.37
L1.44
I1.41
C
PAM
W5.59
Y5.62
R5.60
L1.44
I1.47
I1.48
I1.51
TM1
TM2
TM3
TM4
TM5
TM6
TM7
H8
A
B
C
D
E
D
V1.32
Q1.31
I1.35
L1.38
E
F6.60
V6.57
I6.53
I6.46
F7.34
L7.37
L7.41
I7.44